Chemistry–A European Journal
Research Article
doi.org/10.1002/chem.202201447
Chemistry Europe
European Chemical Societies Publishing
www.chemeurj.org

Chelating Phosphorus–An O, C, O-Coordinating Pincer-Type Ligand Coordinating P^{III} and P^{V} Centres

Michael Gock,[a] Michael Lutter,[a] Anna Pintus,[b] Dieter Schollmeier,[c] Massimiliano Arca,*[b] Vito Lippolis,*[b] and Klaus Jurkschat*[a]

Dedicated to Jutta Zepp on the occasion of her birthday.

Abstract: The sequence of reactions of the phosphorus-containing aryllithium compound 5-*t*-Bu-1,3-[(P(O)(O-*i*-Pr)$_2$]$_2$C$_6$H$_2$Li (ArLi) with Ph_2PCl, $KMnO_4$, elemental sulfur and elemental selenium, respectively, gave the aryldiphenylphosphane chalcogenides 5-*t*-Bu-1,3-[(P(O)(O-*i*-Pr)$_2$]$_2$C$_6$H$_2$P(E)Ph$_2$ (**1**, E = O; **2**, E = S; **3**, E = Se). Compound **1** partially hydrolysed giving [5-*t*-Bu-1-{(P(O)(O-*i*-Pr)$_2$}-3-{(P(O)(OH)$_2$}C$_6$H$_2$]P(O)Ph$_2$ (**4**). The reaction of ArLi with $PhPCl_2$ provided the benzoxaphosphaphosphole [1(P), 3(P)-P(O)(O-*i*-Pr)OPPh-6-*t*-Bu-4-P(O)(O-*i*-Pr)$_2$]C$_6$H$_2$P (**5i**) as a mixture of the two diastereomers. The oxidation of **5i** with elemental sulfur gave the benzoxaphosphaphosphole sulfide [1(P), 3(P)-P(O)(O-*i*-Pr)OP(S)Ph-6-*t*-Bu-4-P(O)(O-*i*-Pr)$_2$]C$_6$H$_2$ (**5**) as pair of enantiomers P1(*R*), P3(*S*)/P1(*S*), P3(*R*) of the diastereomer (*RS/SR*)-**5** (**5b**). The aryldiphenylphosphane 5-*t*-Bu-1,3-[(P(O)(O-*i*-Pr)$_2$]$_2$C$_6$H$_2$PPh$_2$ (**6**) was obtained from the reaction of the corresponding aryldiphenylphosphane sulfide **2** with either sodium hydride, NaH, or disodium iron tetracarbonyl, $Na_2Fe(CO)_4$. The oxidation of the aryldiphenylphosphane **6** with elemental iodine and subsequent hydrolysis yielded the aryldiphenyldioxaphosphorane 9-*t*-Bu-2,6-(O*H*)-4,4-Ph$_2$-3,5-O$_2$-2,6-P$_2$-4λ^5-P-[5.3.1.0]-undeca-1(10),7(11),8-triene (**7**). Both of its diastereomers, (*RR/SS*)-**7** (**7a**) and (*RS/SR*)-**7** (**7b**), were separated as their chloroform and *i*-propanol solvates, **7a**·2CHCl$_3$ and **7b**·*i*-PrOH, respectively. DFT calculations accompanied the experimental work.

Introduction

In recent years, some of the authors reported the syntheses, reactivity and structures of a variety of organosilicon,[1–6] organotin,[7–20] organolead[21, 22] and organobismuth[23] compounds bearing phosphorus-containing O,C,O-coordinating pincer-type ligands (Scheme 1, type **A**). In the course of these studies we learned that the corresponding organoelement cations, for instance obtained by abstraction of a phenyl or hydrogen substituent (R in Scheme 1), gave the corresponding benzoxaphosphasilole,[2, 3] benzoxaphosphastannole,[3, 8, 10] benzoxaphosphaplumbole[21] of type **B** upon reaction with water or a halide anion (Scheme 1). The formation of these benzoxaphospha(semi)metalloles can be rationalized by recognizing the canonical formula of the cation with the formal positive charge located at the phosphorus centre that activates the adjacent O–C bond. The latter undergoes cleavage by nucleophiles such as water and halide anions (Scheme 1). Alternatively, the bismuth representative **C**[23] formed spontaneously in course of the reaction between $BiCl_3$ with [5-*t*-Bu-2,6-{P(O)(OEt)$_2$}$_2$C$_6$H$_2$Li.

All the benzoxaphospha(semi)metalloles have in common the formation of only one pentaatomic C$_2$MPO-heterocycle (M = Si, Sn, Pb), although a second one should be possible including the other (*i*-PrO)$_2$PO phosphorus group. Dostal *et.al.* published the formation of comparable C$_3$EO-heterocycles (E = P, As, Sb) obtained from the reaction of group XV element halides with related N,C,O-coordinating pincer-type ligands (Scheme 2).[24,25] The formation of *t*-BuCl accompanies these reactions. Antimony and bismuth gave also stable cations (Scheme 2).[26a] However, double ring closure by the formation of two E-O bonds has not been observed so far, even though a second potentially leaving group such as a halide at the central element centre and ethers or esters in the pincer-type ligand are present.

Herein, with the aim of expanding our ongoing systematic studies on hypercoordinate main group element compounds, we report the synthesis, structural characterization, and DFT analysis of the chemical bond and electronic structure of a

[a] Dr. M. Gock, Dr. M. Lutter, Prof. Dr. K. Jurkschat
Technische Universität Dortmund
Fakultät für Chemie und Chemische Biologie
44221 Dortmund (Germany)
E-mail: klaus.jurkschat@tu-dortmund.de
[b] Dr. A. Pintus, Prof. Dr. M. Arca, Prof. Dr. V. Lippolis
Dipartimento di Scienze Chimiche e Geologiche
Università degli Studi di Cagliari, S.S. 554
Bivio per Sestu, 09042 Monserrato (CA) (Italy)
E-mail: lippolis@unica.it
marca@unica.it
[c] Dr. D. Schollmeier
Johannes Gutenberg-Universität Mainz
Institut für Organische Chemie
Duesbergweg 10–14, 55099 Mainz (Germany)

Supporting information for this article is available on the WWW under https://doi.org/10.1002/chem.202201447

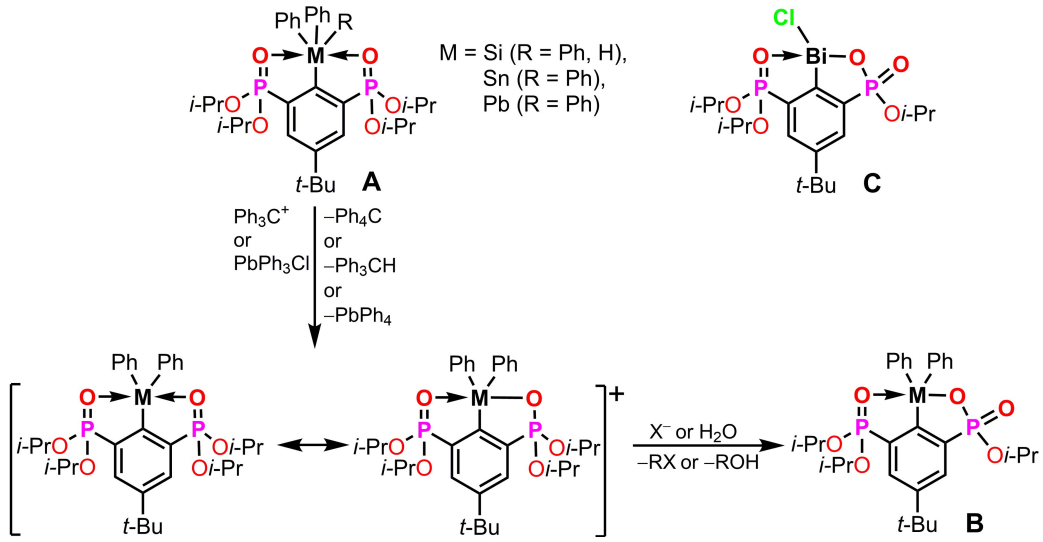

Scheme 1. Synthesis of benzoxaphosphametalloles (X^- = halide anion).

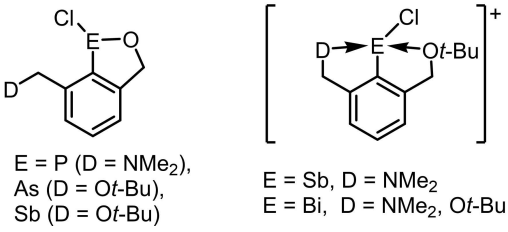

Scheme 2. Group XV element heterocycles and cations.

variety of organophosphorus P^{III} and P^{V} compounds containing the O,C,O-coordinating pincer-type ligand [5-*t*-Bu-1,3-{(P(O)(O-*i*-Pr)$_2$}$_2$C$_6$H$_2$]$^-$. We demonstrate for the first time for this particular pincer-type ligand the possibility of double cyclization at a P centre to afford diastereomeric aryldiphenyldioxaphosphoranes. These are related to Arduengo's ADPO derivatives N[CHC(*t*-Bu)O]$_2$PR$_2$ (ADPO = R-3,7-disubstituted 5-aza-2,8-dioxa-l-phosphabicyclo[3.3.0]octa-2,4,6-triene; R = Cl, Me) showing a trigonal bipyramidal geometry at the 10-P-5 hypercoordinate centre.[26b,c]

Results and Discussion

The reaction of the proligand 5-*t*-Bu-1,3-[(P(O)(O-*i*-Pr)$_2$]$_2$C$_6$H$_3$ with lithium diisopropyl amide followed by addition of chlorodiphenylphosphane and treatment of the in situ-formed aryldiphenylphosphane RPPh$_2$ with potassium permanganate, KMnO$_4$, elemental sulfur, or elemental selenium provided the corresponding aryldiphenylphosphane oxide RP(O)Ph$_2$ (**1**, as its toluene solvate **1**·0.5 C$_7$H$_8$), aryldiphenylphosphane sulfide RP(S)Ph$_2$ (**2**), and aryldiphenylphosphane selenide RP(Se)Ph$_2$ (**3**), (R = 5-*t*-Bu-1,3-[(P(O)(O-*i*-Pr)$_2$]$_2$C$_6$H$_2$), respectively, as either colourless (**1**, **2**) or yellow (**3**) crystalline materials in moderate yields (Scheme 3) [see Supporting Information for synthetic details and spectroscopic characterization: Figures S1-S20 for **1**·0.5 C$_7$H$_8$; Figures S22–S43 for **2**; Figures S44-S56 for **3**].

Single crystals suitable for X-ray diffraction analysis were isolated for compound **1**, as its toluene solvate **1**·0.5 C$_7$H$_8$, **2**, and **3** (Figures 1–3, Table S1 in Supporting Information).

The aryldiphenylphosphane oxide toluene solvate **1**·0.5 C$_7$H$_8$ crystallized in the triclinic space group $P\bar{1}$ with two pairs of independent molecules in the unit cell. Both differ only slightly in their interatomic distances and angles. Consequently, the structure of only one molecule is discussed in detail. The P1 centre is four-coordinated by C2, O1, O1′, O1″ and exhibits a distorted tetrahedral geometry with angles ranging between 116.92(11) [O1-P1-O1″] and 101.76(10)° [O1′-P1-O1″]. For P2, the distortion from ideal tetrahedral geometry is even more pronounced, with angles ranging between 119.44(10) [O2-P2-O2″] and 98.30(9)° (O2′-P2-O2″). The origin of this distortion is O3 approaching P2 via the tetrahedral face defined by O2, O2″, and C6 at a distance of 2.896(2) Å. This distance is considerably shorter than the sum of the van der Waals radii of the atoms involved (Σr_{vdW} = 3.60 Å)[27] and renders the P2 centre [4 + 1]-coordinated. The slightly longer P3-O3 distance of 1.4800(18) Å as compared to the P1-O1 distance of 1.4553(18) Å (O1 is not involved in any further interaction than with P1) also reflects the O3→P2 interaction. In addition, the C6-C1-P3 and C2-C1-P3 angles of 115.89(19) and 126.01(19)°, respectively, deviate from 120° and hint at an O3→P2 attraction. The P3 centre also shows a distorted tetrahedral coordination environment with angles ranging between 106.96(11) (O3-P3-C1) and 112.45(12)° (O3-P3-C31). The O2 donor approaches the P3 centre via the tetrahedral face defined by C1, C31, O3 at a distance of 3.224(2) Å and makes P3 [4 + 1]-coordinated.

Both the aryldiphenylphosphane sulfide **2** and the corresponding selenide **3** crystallized in the monoclinic space group $P2_1/m$ with two molecules in the unit cell. The geometry about the P1 centres is again distorted tetrahedral with angles ranging between 100.82(15) (O1′-P1-O1″, **3**) and 118.31(9)° (O1-P1-O1″,

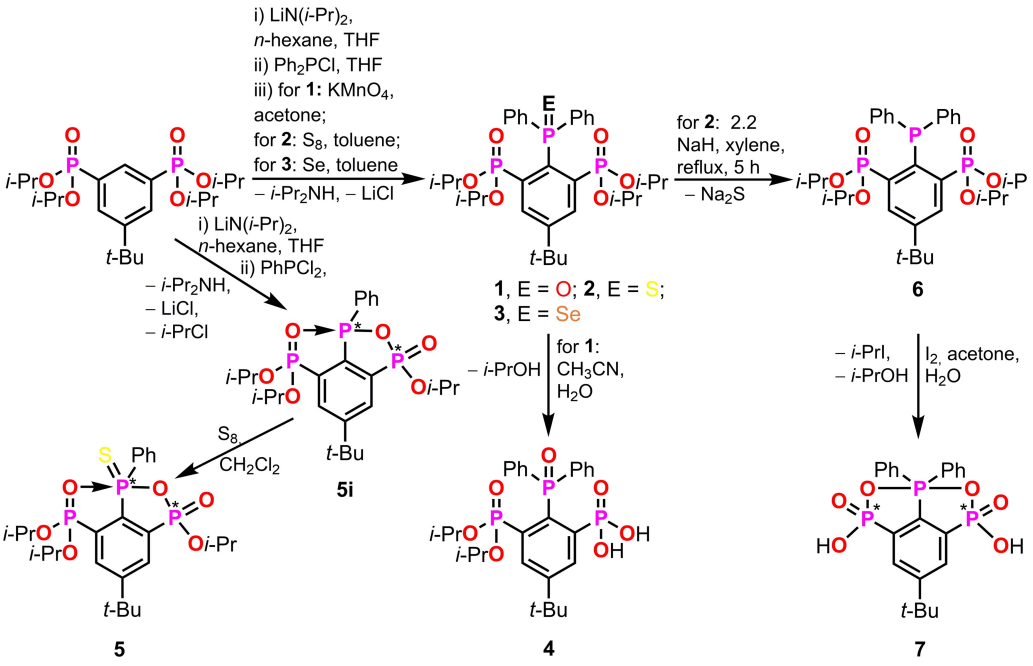

Scheme 3. Syntheses of compounds **1**–**7**. The compounds **5**, **5i**, and **7** contain two stereogenic centres each (indicated by asterisks) and exist as two diastereomers.

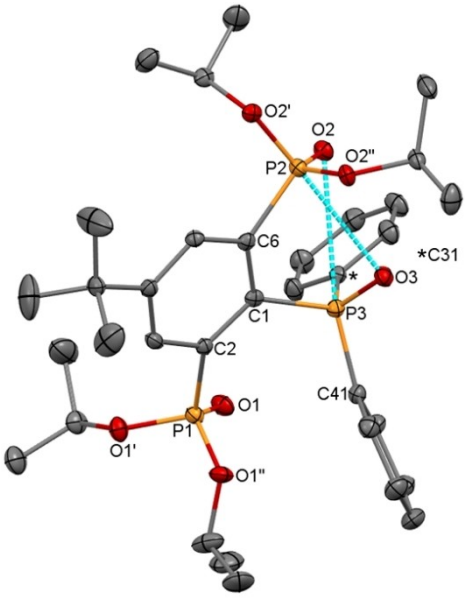

Figure 1. Molecular structure of the aryldiphenylphosphane oxide **1** isolated as the toluene solvate **1**·0.5C_7H_8 (one of the two independent molecules). The toluene solvate molecule is omitted for clarity. Figure S21 (Supporting Information) shows the complete structure. Displacement ellipsoids are drawn at 30% probability level. Hydrogen atoms were omitted for clarity. Selected interatomic distances (Å): P1-O1 1.4553(18), P1-O1′ 1.5755(19), P1-O1′′ 1.5665(19), P2-O2 1.4624(17), P2-O2′ 1.5852(17), P2-O2′′ 1.5702(18), P2-O3 2.896(2), P3-O2 3.224(2), P3-O3 1.4800(18). Selected interatomic angles (°): P1-C2-C1 125.92(19), O2-P2-O2′ 113.52(10), O2-P2-O2′′ 119.44(10), O2-P2-C6 115.11(11), O2′-P2-O2′′ 98.30(9), O2′-P2-C6 102.86(10), O2′′-P2-C6 105.16(11), O2′-P2-O3 169.95(10), P2-C6-C1 125.44(19), O2-P3-C41 170.16(19), O3-P3-C1 106.96(11), O3-P3-C31 112.45(12), O3-P3-C41 107.30(12), C1-P3-C31 111.99(12), C1-P3-C41 110.67(12), C2-C1-P3 126.01(19), C6-C1-P3 115.89(19).

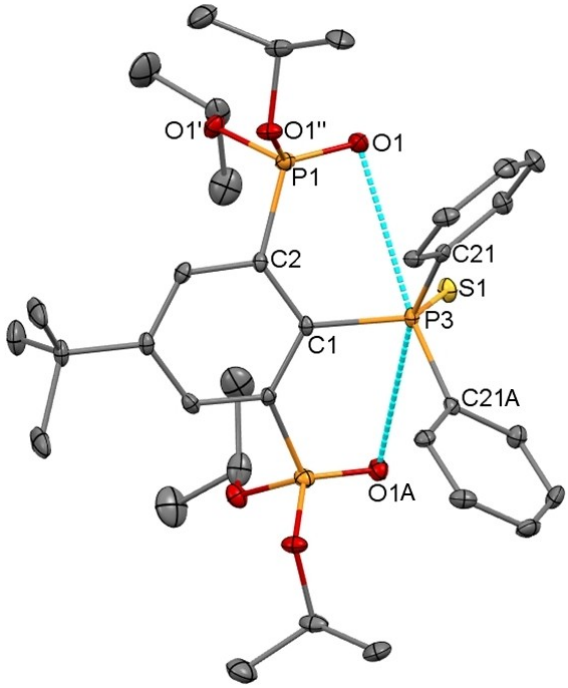

Figure 2. Molecular structure of the aryldiphenylphosphane sulfide **2**. Displacement ellipsoids are drawn at 30% probability level. Hydrogen atoms were omitted for clarity. Selected interatomic distances (Å): P1-O1 1.4575(15), P1-O1′ 1.5878(15), P1-O1′′ 1.5694(13), P3-O1 3.195(3), P3-S1 1.9415(10), Selected interatomic angles (°): P1-C2-C1 126.92(17), C1-P3-S1 114.22(9), C1-P3-C21 106.56(9), C21-P3-S1 115.10(7), C21-P3-C21A 97.67(12), C2-C1-P3 121.38(13), S1-P3-C21 115.10(7), O1-P3-C21A 161.65(2), O1-P3-O1A 133.87(9).

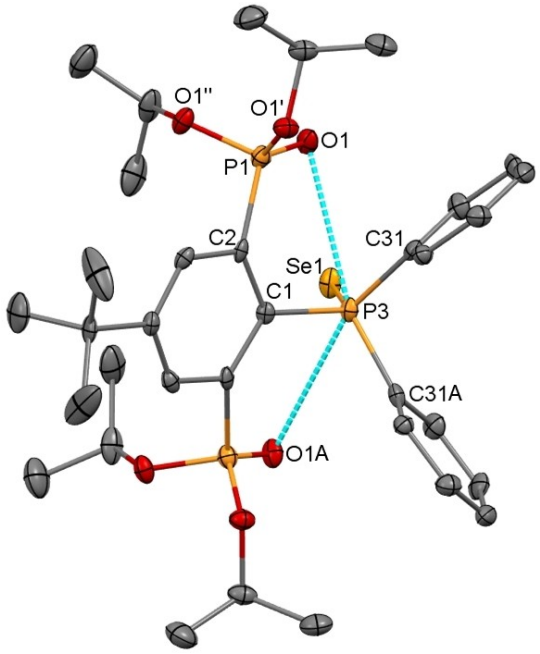

Figure 3. Molecular structure of the aryldiphenylphosphane selenide **3**. Displacement ellipsoids are drawn at 30% probability level. Hydrogen atoms were omitted for clarity. Selected interatomic distances (Å): P1-O1 1.463(3), P1-O1′ 1.560(3), P1-O1′′ 1.582(3), P3-O1 3.195(3), P3-Se1 2.0952(17). Selected interatomic angles (°):P1-C2-C1 128.39(3), C1-P3-Se1 113.84(17), C1-P3-C31 106.79(17), C31-P3-C31 A 98.7(2), Se1-P3-C31 114.68(15), O1-P3-C31 A 161.25(16), O1-P3-O1 A 135.73(15).

2). The same holds for P3 with angles ranging between 97.67(12) (C21-P3-C21A, **2**) and 115.10(7) (S1-P3-C21, **2**). The O1 and O1A donor centres approach P3 via the tetrahedral faces defined by C1, C21, S1 and C1, C21A, S1 (for **2**), and C1, C31, Se1 and C1, C31A, Se1 (for **3**) at equal distances of 3.195(3) Å. These distances are shorter than the sum of the van der Waals radii[27] of the atoms involved (see above).

^{31}P NMR spectra of $CDCl_3$ solutions of **1**, **2**, and **3** (Supporting Information, Figures S17–S19, S40–S42, S53–S55) show triplet resonances for the $P(O)Ph_2$, $P(S)Ph_2$, and $P(Se)Ph_2$ phosphorus centres at δ 37.40 [$^3J(^{31}P–^{31}P) = 11$ Hz], 49.46 [$^3J(^{31}P–^{31}P) = 11$ Hz, $^1J(^{31}P–^{13}C) = 90$ Hz], and 38.11 ppm [t, $^3J(^{31}P–^{31}P) = 10$ Hz, $^1J(^{31}P–^{77}Se) = 763$ Hz], respectively, and doublet resonances for the $P(O)(O\text{-}i\text{-}Pr)_2$ phosphorus centres at δ 14.78 ($^3J(^{31}P–^{31}P) = 11$ Hz, **1**], 13.13 [$^3J(^{31}P–^{31}P) = 11$ Hz, $^1J(^{31}P–^{13}C) = 188$ Hz, **2**], and 12.67 ppm [$^3J(^{31}P–^{31}P) = 10$ Hz, **3**] with the expected integral ratios of 1:2. These data indicate symmetric structures in solution even for compound **1**. Apparently, the P=O→P(O)Ph$_2$ and P=O→P(O)(O-*i*-Pr)$_2$ interactions noticed for **1** in the solid state is kinetically labile in solution or even absent. The parent triphenylchalcogenides $P(E)Ph_3$ lacking the potential P(O)(O-*i*-Pr)$_2$ donor substituents show ^{31}P NMR chemical shifts of δ 28 (E = O), 43 (E = S), and 35 ppm (E = Se) being close to the chemical shifts of **1**–**3**. This supports the conclusion that in solution there are no or rather weak intramolecular donor-acceptor interactions. The ^{1}H and ^{13}C NMR spectra are as expected (Supporting Information, Figures S1–S16, S22–S39, S44–S52). Exemplarily, a ^{1}H NMR spectrum of a solution of the aryldiphenylphosphane sulfide **2** in $CDCl_3$ shows two doublet resonances at δ 0.92 [$^3J(^1H–^1H) = 6$ Hz] and 1.20 ppm [$^3J(^1H–^1H) = 6$ Hz, $^1J(^1H–^{13}C) = 45$ Hz] assigned to the $CH(CH_3)_2$ protons, a singlet resonance at δ 1.42 ppm assigned to the $C(CH_3)_3$ protons, and a septet resonance at δ 4.38 ppm [($^3J(^1H–^1H) =$ 6 Hz] assigned to the $CH(CH_3)_2$ protons. The signal for the *ortho* protons H_o of the phenyl substituents appears as a complex pattern centred at δ 7.76 ppm, and those for the *meta* and *para* protons H_m and H_p show a superimposed complex pattern centred at δ 7.32 ppm. Finally, the C_6H_2 protons show a AA'XX'-type resonance centred at δ 8.02 ppm [$^3J(^1H–^{31}P) = 20$ Hz, $^4J(^1H–^{31}P) = 4$ Hz]. A ^{13}C NMR spectrum reveals two resonances for the $CH(CH_3)_2$ carbon atoms, one signal for the $CH(CH_3)_2$ carbon atoms, two signals for the *t*-butyl substituents, four signals for the phenyl carbon atoms and four resonances for the aryl carbon atoms. Electrospray ionization mass spectrometry (ESI MS, positive mode) revealed the identities of **2** and **3** as well. They show peaks at m/z 679.3 and 727.3, respectively, being assigned to the corresponding protonated molecular ions. An ESI mass spectrum of **1** showed a major intense peak at m/z 561.1 that is tentatively assigned to $[M–C_3H_6–C_3H_7O^-]^+$.

Serendipitous isolation of a partial hydrolysis product of 1

In one of the numerous attempts of growing single crystals for compound **1**, the latter was dissolved in acetonitrile and the solution obtained was left for slow evaporation under non-inert conditions. Surprisingly, partial hydrolysis of one phosphonyl moiety took place giving [5-*t*-Bu-1-{(P(O)(O-*i*-Pr)$_2$}-3-{(P(O)(OH)$_2$}C_6H_2]P(O)Ph$_2$ (**4**) as colourless single crystalline material (Figure 4, Table S1 in Supporting Information).

The partially hydrolysed aryldiphenylphosphane oxide **4** crystallized in the triclinic space group $P\bar{1}$ with two molecules in the unit cell. The geometry about the P1 centre resembles those of the P1 centres of compounds **2** and **3** with angles varying between 99.54(9) (O1′-P1-C2) and 117.01(9)° (O1-P1-O1′). For P2, the variation of the angles is narrower and ranges between 106.22(10) (O2′′-P2-C6) and 114.39(9)° (O2-P2-O2′′). The P2···O3 distance of 2.936(2) Å renders P2 [4 + 1]-coordinated. This distance is shorter than the corresponding distance in its related derivative **1** (see above). The origin of this shortening is the intramolecular unsymmetrical O2′-H2′···O3 hydrogen bridge with an O2′···O3 distance of 2.478(2) Å that causes the O3 to get closer to P2. The P3 centre is also [4 + 1]-coordinated with O1 approaching P3 via the tetrahedral face defined by C1, C31, and C41 at a distance of 3.024(2) Å. This distance is shorter than the corresponding distances in compounds **2** and **3**.

In addition to the intramolecular O2′-H2′···O3 hydrogen bridge, the intermolecular O2′′-H2′′···O2A and the symmetry-related O2′′A-H2′′A···O2 hydrogen bridges [O2···O2′′A = 2.503(2) Å] origin a centrosymmetric dimer (Figure 4, right, Table 1).

A ^{31}P NMR spectrum (Supporting Information, Figures S57–S59) of a solution of **4** in $CDCl_3$ shows a pseudo triplet

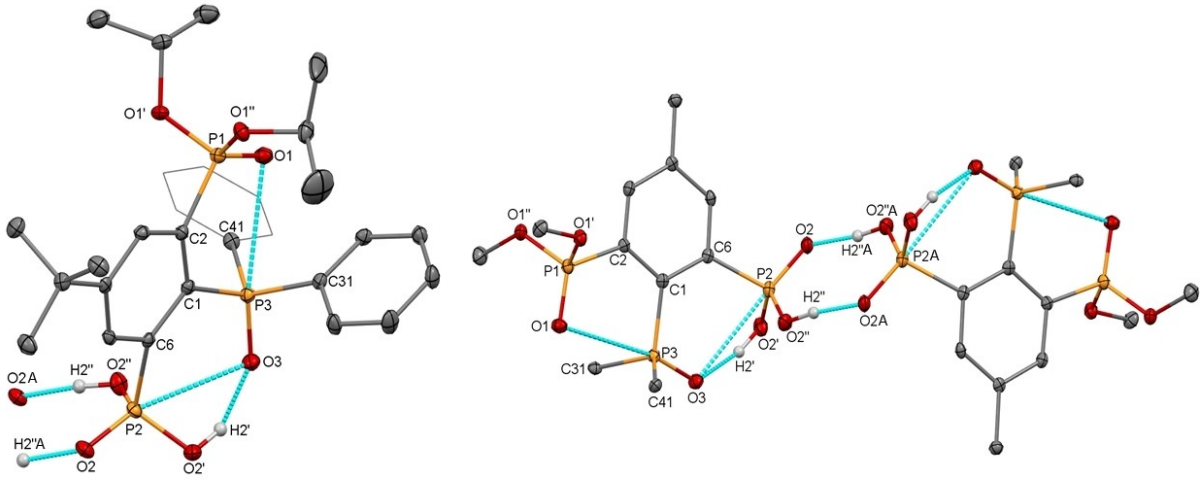

Figure 4. Molecular structure of compound **4** (left: complete molecule, right: simplified image of the hydrogen-bridged dimer with the methyl groups omitted, and only the C_{ipso} carbon atoms of the phenyl substituents shown). Displacement ellipsoids are drawn at 30 % probability level. Hydrogen atoms were omitted for clarity with the exception of those involved in O-H···O hydrogen bonds. Selected interatomic distances (Å): P1-O1 1.4606(16), P1-O1′ 1.5715(15), P1-O1″ 1.5687(17), P2-O2 1.5099(15), P2-O2′ 1.5553(16), P2-O2″ 1.5206(18), P2-C6 1.831(2), P2-O3 2.936(2), P3-O1 3.024(2), P3-O3 1.4980(16). Selected interatomic angles (°): O1-P1-O1′ 117.01(9), O1-P1-O1″ 114.64(9), O1-P1-C2 114.29(10), O1′-P1-O1″ 102.62(9), O1′-P1-C2 99.54(9), O1″-P1-C2 106.99(10), C1-C2-P1 125.67(16), O2-P2-O2′ 107.45(9), O2-P2-O2″ 114.39(9), O2-P2-C6 108.05(10), O2-P2-O3 164.82(11), O2′-P2-O2″ 111.20(10), O2′-P2-C6 109.43(9), O2″-P2-C6 106.22(10), C1-C6-P2 127.36(18), C1-P3-C31 107.53(10), C1-P3-C41 109.54(10), C1-P3-O1 79.70(9), C1-P3-O3 111.21(9), C31-P3-C41 114.53(10), O1-P3-O3 168.89(9), C2-C1-P3 123.00(16).

Table 1. Interatomic distances (Å) and angles (°) for the hydrogen bridges in compound **4**.

D-H···A	d(D-H)	d(H···A)	d(D···A)	(DHA)
O2′-H2′···O3	0.86(2)	1.67(2)	2.478(2)	156(3)
O2″-H2″···O2 A[i]	0.89(2)	1.62(3)	2.503(2)	171(3)

[i] Symmetry transformations used to generate equivalent atoms: -x, 1-y, 1-z.

resonance at δ 54.2 ppm [$^3J(^{31}P\text{-}^{31}P) = 5$ Hz] assigned to the $P(O)Ph_2$ phosphorus atom (see Figure S60 for the ESI-mass spectrum of **4**). This resonance is considerably low-field shifted as compared to the signal of the corresponding phosphorus atom in the related non-hydrolyzed aryldiphenylphosphane oxide **1**, despite the fact that **1** and **4** differ only by the replacement of two *iso*-propoxy substituents in **1** by two OH substituents in **4**. With caution we trace this considerable difference to the P=O···H–O-P hydrogen bridges observed for **4** in the solid state (see Figure 4) being retained in solution. The observation in an ESI MS of a peak at m/z 1037.2 that satisfactorily fits with $C_{50}H_{59}O_{12}P_6$ supports this interpretation. The signals assigned to the $P(O)(O\text{-}i\text{-}Pr)_2$ and $P(O)(OH)_2$ phosphorus atoms appear as pseudo-triplet resonances at δ 15.2 [$^3J(^{31}P\text{-}^{31}P) = 5$ Hz] and 14.1 ppm [$^3J(^{31}P\text{-}^{31}P) = 5$ Hz], respectively.

From the experimental data at hand, the reason for the hydrolysis of only one of the two phosphonyl groups instead of a statistical distribution of OH groups at both of these is not clear yet. Notably, a solution of the phosphane sulfide derivative **2** in CH_3CN containing some droplets of water did not show any hydrolysis of the phosphonyl moieties after stirring the mixture for four days at room temperature.

The subsequent reaction of the proligand 5-*t*-Bu-1,3-[(P(O)(O-*i*-Pr)$_2$]$_2$C$_6$H$_3$ with LiN(*i*-Pr)$_2$ and $PhPCl_2$ gave a reaction mixture whose ^{31}P NMR spectrum (Supporting Information, Figures S61–S64) showed two sets of three signals with an integral ratio 3:2. These signals can be attributed to the two diastereomers of the benzoxaphosphaphosphole [1(P), 3(P)-P(O)(O-*i*-Pr)OPPh-6-*t*-Bu-4-P(O)(O-*i*-Pr)$_2$]C$_6$H$_2$ (**5i**) (Scheme 3). The diastereomeric mixture of **5i** was isolated as a solid material (see Supporting Information for synthetic details and ^{31}P NMR spectroscopic characterization). However, any attempts at separating the diastereomers (*RR*/*SS*)-**5i** (**5ia)** and (*RS*/*SR*)-**5i** (**5ib)** failed.

The subsequent reaction of the proligand 5-*t*-Bu-1,3-[(P(O)(O-*i*-PrO)$_2$]$_2$C$_6$H$_3$ with LiN(*i*-Pr)$_2$, $PhPCl_2$, and elemental sulphur provided after the workup procedure the benzoxaphosphaphosphole sulfide diastereomer [1(P),3(P)-P(O)(O-*i*-Pr)OP(S)Ph-6-*t*-Bu-4-P(O)(O-*i*-Pr)$_2$]C$_6$H$_2$, (*RS*/*SR*)-**5** (**5b**), as a colourless crystalline material (Scheme 3) [see Supporting Information for synthetic details and spectroscopic characterization of **5b**: Figures S65–S90]. Compound **5b** is stable under non-inert conditions and shows good solubility in CH_2Cl_2 and $CHCl_3$. It is less soluble in diethyl ether and almost insoluble in *n*-hexane. A ^{31}P NMR spectrum of a solution of **5b** in $CDCl_3$ revealed one set of three signals indicating the presence of only one diastereomer. Despite intensive efforts, the second diastereomer (*RR*/*SS*)-**5** (**5a**) was not found. Apparently, it was either lost during the workup procedure or, as result of the relatively bulky sulfur substituent, not formed. This was not investigated further experimentally. Calculations reveal both diastereomers being very close in energy (see below). A ^{31}P NMR spectrum of **5b** did not change in time indicating that no epimerization took place under the given experimental conditions. Notably, the related

benzoxaphosphasilole [1(P), 3(Si)-P(O)(OEt)OSiMePh-6-*t*-Bu-4-P-(O)(OEt)$_2$]C$_6$H$_2$ undergoes a *p*-MeC$_6$H$_4$SO$_3$H-catalyzed epimerization in C$_6$D$_6$ solution.[2]

The benzoxaphosphaphosphole sulphide diastereomer **5b** crystallized in the monoclinic space group $P2_1/n$ with four molecules in the unit cell (Table S1 in Supporting Information). In the structure, both enantiomers P1(*R*), P3(*S*) and P1(*S*), P3(*R*) of the diastereomer **5b** are present (see Figure 5 for the former), with P1 and P3 being stereogenic centres. Both of these phosphorus centres are part of an almost planar five-membered C$_2$POP ring with torsion angles ranging between 10.66(16) [P1-O1′-P3-C1] and −9.19(17)° [C2-P1-O1′-P3]. The P1 as well as the P2 centre show each a distorted tetrahedral environment with angles ranging between 97.51(11) [O1′-P1-C2] and 118.44(14)° [O1-P1-C2]. The P3 centre, analogously to the P3 centres of the aryldiphenylphosphane oxides **1** and **4**, exhibits a [4+1]-coordination in which O2 approached the P3 via the tetrahedral face defined by C1, C31, and S1 at a distance of 3.012(2) Å. This interaction can be tentatively considered electrostatic in nature, since the P2-O2 distance of 1.453(2) Å is exactly the same as the P1-O1 distance [1.453(2) Å] with O1 only bound to P1 and not being involved in any additional O→P interaction.

A ^{31}P NMR spectrum (Supporting Information, Figures S84–S86) of a solution of **5b** in C$_6$D$_6$ is in line with the molecular structure as established by single crystal X-ray diffraction analysis for the solid state. It shows three resonances at δ 12.6 ppm ["t", $^3J(^{31}P\text{-}^{31}P) = 6$ Hz, *P*(O)(O-*i*-Pr)$_2$], 17.2 (dd, $^3J(^{31}P\text{–}^{31}P) = 8$ Hz, $^3J(^{31}P\text{–}^{31}P) = 12$ Hz, *P*(O)(OP)(O-*i*-Pr)], and 82.0 [dd, $^3J(^{31}P\text{–}^{31}P) = 7$ Hz, $^3J(^{31}P\text{–}^{31}P) = 12$ Hz, *P*(S)(OP)Ph], respectively. As result of the *P*(S) phosphorus being a stereogenic centre, the CH(CH_3)$_2$ methyl protons become diastereotopic giving, in its ^{1}H NMR spectrum (Supporting Information, Figures S65–S68 including a drawing with numbering of the H atoms discussed below), six doublet resonances at δ 0.745, 0.975, 0.985, 1.125, 1.195, and 1.245 ppm with each showing a $^3J(^1H\text{-}^1H)$ coupling constant of 5 Hz. The $CH(CH_3)_2$ protons appear as two complex patters centred at δ 4.08 (integral 1) and 4.98 ppm (integral 2), respectively. A ^{1}H-^{1}H COSY NMR spectrum reveals the two doublets at δ 0.745 and 0.975 ppm and the complex pattern at δ 4.08 ppm belonging to the P(O)(OP)O$CH(CH_3)_2$ protons H^a, H^b, and H^c, whereas the remaining four doublets and the complex pattern at δ 4.98 ppm belong to the P(O)[O$CH(CH_3)_2$]$_2$ protons H^d–H^h. The *t*-butyl protons C(CH_3) appear as a singlet resonance at δ 0.97 ppm, the phenyl protons H$_o$ as complex pattern centred at δ 8.36 ppm, and the H$_m$ and H$_p$ protons at δ 6.99 ppm. The H^i and H^j protons show a doublet of doublets resonance at δ 8.22 ppm [$^3J(^1H\text{-}^{31}P) = 15$ Hz, $^4J(^1H\text{-}^{31}P) = 5$ Hz] and a doublet resonance at δ 8.13 ppm [$^3J(^1H\text{-}^{31}P) = 10$ Hz]. In addition to the ^{1}H NMR resonances discussed above, the spectrum reveals additional low intense $CH(CH_3)_2$ complex pattern-signals of different integral at δ 4.765 ppm (integral 0.49) and δ 4.270 ppm (integral 0.08). The former shows cross peaks with two doublet resonances at δ 1.075 ppm [$^3J(^1H\text{-}^1H)$ 5 Hz] and δ 1.230 ppm [$^3J(^1H\text{-}^1H)$ 5 Hz] and the latter with resonances at 0.83 and 1.04 ppm. In the region for the aromatic protons, there are minor intense complex pattern-resonances as well. With caution, we assign these additional resonances to species related to **5b**; possibly products of ongoing hydrolysis.

An ESI mass spectrum (Supporting Information, Figure S90) shows a major intense peak at m/z 559.1 which is assigned to the protonated molecular ion $[M+H]^+$ of **5b**.

The reaction in xylenes at reflux of the aryldiphenylphosphane sulfide **2** with sodium hydride gave the corresponding aryldiphenylphosphane **6** as a yellow solid in high yield (Scheme 3) (see Supporting Information for synthetic details and spectroscopic characterization of **6**: Figures S91–S116). Alternatively, compound **6** was also obtained from the reaction between the aryldiphenylphosphane sulfide **2** and a slight excess (ratio 1:1.2) of disodium iron tetracarbonyl, Na$_2$Fe(CO)$_4$. It dissolves well in common organic solvents such as CH_2Cl_2, THF, diethylether, toluene, but it is sparingly soluble in hexanes.

Recrystallization of **6** from *n*-hexane at -20 °C provided colourless single crystals suitable for X-ray diffraction analysis. Figure 6 shows the molecular structure of **6**.

The aryldiphenylphosphane **6** crystallized in the monoclinic space group $P2_1/c$ with four molecules in the unit cell (Table S1 in Supporting Information). As discussed for the P^V derivatives **1**–**3**, the P1 and P2 centres show distorted tetrahedral environments with angles ranging between 117.78(8) [O1-P1-O1′] and 96.85(7)° [O1′-P1-O1″]. At a first sight, the P3 centre exhibits a trigonal pyramidal environment with C-P-C angles falling in the narrow range between 105.42(8) (C1-P3-C41) and 109.23(9)° (C31-P3-C41). A closer inspection of the structure reveals the P3-O1 [3.338(13) Å], P3-O2 [3.245(13) Å], and P3-O2″ [3.237(13) Å] distances being shorter than the sum of the van der Waals radii[27] of the atoms involved (see above). These distances are in the same range as the P3-O1 distances in the aryldiphenylphosphane sulfide **2** and selenide **3**, and the P3-O2 distance in

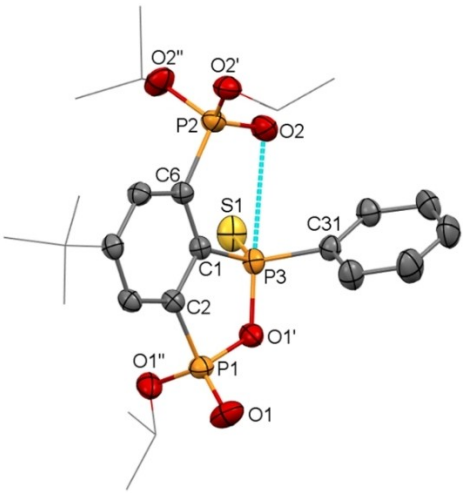

Figure 5. Molecular structure of the benzoxaphosphaphosphole sulphide diastereomer **5b** (the P1(*R*),P3(*S*) enantiomer is shown). The displacement ellipsoids are drawn at 30% probability level. For the sake of clarity, the *t*-butyl and *i*-propyl substituents are shown as wireframe and the hydrogen atoms were omitted. Selected interatomic distances (Å): P1-O1 1.453(2), P1-O1′ 1.603(2), P1-O1″ 1.559(2), P2-O2 1.453(2), P2-O2′ 1.577(2), P2-O2″ 1.556(2), P3-O1′ 1.641(2), P3-O2 3.012(2), P3-S1 1.9180(10). Selected interatomic angles (°): O1′-P1-C2 97.51(11), C1-P3-C31 110.27(11), C1-P3-S1 117.48(9), C31-P3-S1 117.90(9), O1′-P3-O2 165.43(13).

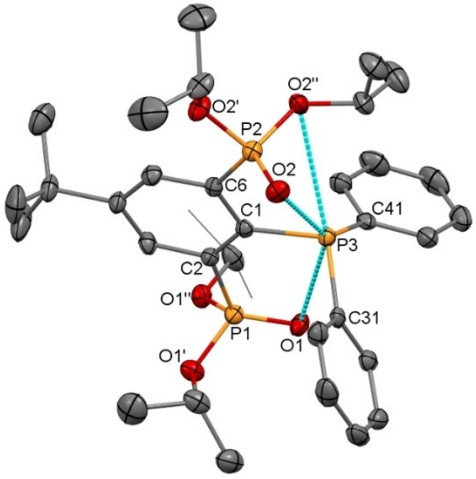

Figure 6. Molecular structure and atom numbering scheme of the aryldiphenylphosphane **6**. Displacement ellipsoids are drawn at 30% probability level. For the sake of clarity, the methyl groups of one *i*-Pr substituent are shown as wireframe, and the hydrogen atoms were omitted for clarity. Selected interatomic distances (Å): P1-O1 1.4514(13), P1-O1′ 1.5669(13), P1-O1′′ 1.5723(13), P2-O2 1.4593(13), P2-O2′ 1.5782(13), P2-O2′′ 1.5739(13), P3-O1 3.338(13), P3-O2 3.245(13), P3-O2′′ 3.237(13). Selected interatomic angles (°): C1-C2-P1 128.85(14), C1-C6-P2 121.49(14), C1-P3-C31 105.72(8), C1-P3-C41 105.42(8), C31-P3-C41 109.23(9), C1-P3-O2 80.01(6), C1-P3-O2′′ 78.51(7), C31-P3-O2 97.39(7), C31-P3-O2′′ 143.18(7), C41-P3-O2 149.72(7), C41-P3-O2′′ 104.49(7), O2-P3-O2′′ 46.52(7).

the related oxide **1** (see above). The O1 atom in **6** approaches the P3 via the face defined by C1, C31, and C41. The O2 and O2′′ contact to P3 from the opposite site with an O2-P3-O2′′ angle of 46.52(7)° (Supporting Information, Figure S117). While the C1-C6-P2 angle of 121.49(14) is close to 120°, the C1-C2-P1 angle of 128.85(14)° suggests the O1-P3 interaction might also be dependent on steric effects. The optimized structure for the aryldiphenylphosphane **6** also shows different values for the C-C-P angles in questions, very close to the experimental ones. Nevertheless, we believe that the reason behind the widening in the C1-C2-P1 angle is to be found in the steric hindrance of the phenyl rings facing the P1=O1 moiety rather than electrostatic repulsion. The long distance of 3.338(13) Å between O1 and P3 seems in fact to prevent this sort of interaction.

A ^{31}P NMR spectrum (Supporting Information, Figures S103–S105) of a solution of **6** in $CDCl_3$-solution revealed a doublet and a triplet resonance at δ 15.7 ppm [$^3J(^{31}P\text{-}^{31}P) = 5$ Hz, *P*(O)(O-*i*-Pr)$_2$] and 0.0 ppm [$^3J(^{31}P\text{-}^{31}P) = 5$ Hz, *P*Ph$_2$] with an integral ratio of 2:1. The chemical shift of the *P*Ph$_2$ phosphorus centre is close to the chemical shift of the phosphorus centre in pseudo tetrahedral PPh$_3$ (δ −5 ppm) indicating no P=O→P coordination. The ^{1}H and ^{13}C NMR spectra (Supporting Information, Figures S91-S102) are as expected and do not show any particularities. An ESI mass spectrum (Supporting Information, Figure S116) reveals the identity of **6** showing a peak at m/e 647.3 which is assigned to $[M+H^+]^+$.

The reaction in acetone under non-inert conditions of the aryldiphenylphosphane **6** with molecular diiodine, I_2, gave a deep-red solution from which the aryldiphenyldioxaphosphorane **7** separated as a colourless precipitate (Scheme 3) (see Supporting Information for synthetic details and spectroscopic characterization: Figures S118–S127). The precipitate consisted of two diastereomers, as it was revealed by a ^{31}P NMR spectrum of its solution in $CDCl_3$ showing two sets of signals at $\delta = 11.3$ [d, $J(^{31}P\text{-}^{31}P)$ 10 Hz] and $\delta = -52.1$ ppm [t, $J(^{31}P\text{–}^{31}P)$ 10 Hz], and $\delta = 11.25$ [d, $J(^{31}P\text{–}^{31}P)$ 10 Hz] and $\delta = -53.60$ ppm [t, $J(^{31}P\text{–}^{31}P)$ 10 Hz]. The integral ratio of these two sets of signals is approximately 2:1 (Supporting Information, Figures S120–S122). The signal at $\delta = -53.60$ ppm is superimposed by another low-intensity triplet resonance at $\delta = -53.65$ ppm (t, $J(^{31}P\text{–}^{31}P)$ 10 Hz), which was not assigned. A ^{1}H NMR spectrum revealed the absence of $CH(CH_3)_2$ protons. Apparently, under the actual experimental conditions, hydrolysis of the ester function took place. The phosphorus centres in *ortho* position to the central P atom are stereogenic. From the NMR data at hand, there was no sign for epimerization of the diastereomers.

The aryldiphenylphosphane **6** was also reacted with molecular dibromine, Br_2, in benzene under non-inert conditions. A ^{31}P NMR spectrum (see Supporting Information, Figure S127) of the crude reaction mixture revealed the same picture as obtained from the reaction with molecular diiodine, i.e., formation of the two diastereomers of **7**, namely (*RR/SS*)-**7** (**7a**) and (*RS/SR*)-**7** (**7b**).

The two diastereomers obtained from the reaction of **6** with I_2 (see above) were separated by fractional crystallization. Single crystals of the diastereomer chloroform solvate **7a**·2$CHCl_3$ (pair of enantiomers *RR/SS*) suitable for X-ray diffraction analysis crystallized from $CHCl_3$ solution. Figure 7 shows the molecular structure. Table 1 contains selected interatomic distances and angles. The aryldiphenyldioxaphosphorane diastereomer **7a**·2$CHCl_3$ (*RR/SS*) crystallized in the orthorhombic space group *Pca*2$_1$ with four asymmetric units in the unit cell (Table S1 in Supporting Information). The asymmetric unit contains a pair of enantiomers (*RR/SS*), which cannot undergo inversion due to the co-crystallized $CHCl_3$ solvate molecules. These solvate molecules render the two enantiomers crystallographically independent.

The phosphorus centres P1, P2, P4, and P5 show each a distorted tetrahedral environment with angles ranging between 115.2(3) (O1-P1-C2) and 97.0(3)° (O1′-P1-C2). The P-O distances involving the terminal oxygen atoms O1 to O4 [range 1.481(6)–1.500(5)] are shorter than the P-O distances involving the phosphorus atoms P1, P2, P4 and P5 atoms with values ranging between 1.573(5) (P1-O1′) and 1.515(6) Å (P2-O2′′). Among these, the distances involving the protonated O1′′ to O4′′ are shorter than the distances to the oxygen atoms within the oxygen atoms O1′ to O4′ that are part of the POPCC five-membered rings. The P3 and P6 centres are both pentacoordinated and exhibit each a trigonal bipyramidal coordination geometry with the oxygen atoms O1′ and O2′ (at P3), and O3′ and O4′ (at P6) occupying the axial, and the C_{ipso} carbon atoms C11 and C21 (at P3), and C41 and C51 (at P6) of the phenyl substituents occupying the equatorial positions. The O1′-P3-O2′ and O3′-P6-O4′ angles of 175.5(3) and 174.1(3)°, respectively, differ from 180° and illustrate the distortion from the ideal trigonal bipyramidal geometry. The axial P3-O1′/O2′ and P6-O3′/O4′ distances of 1.756(4)/1.789(4) and 1.762(4)/1.801(4) Å,

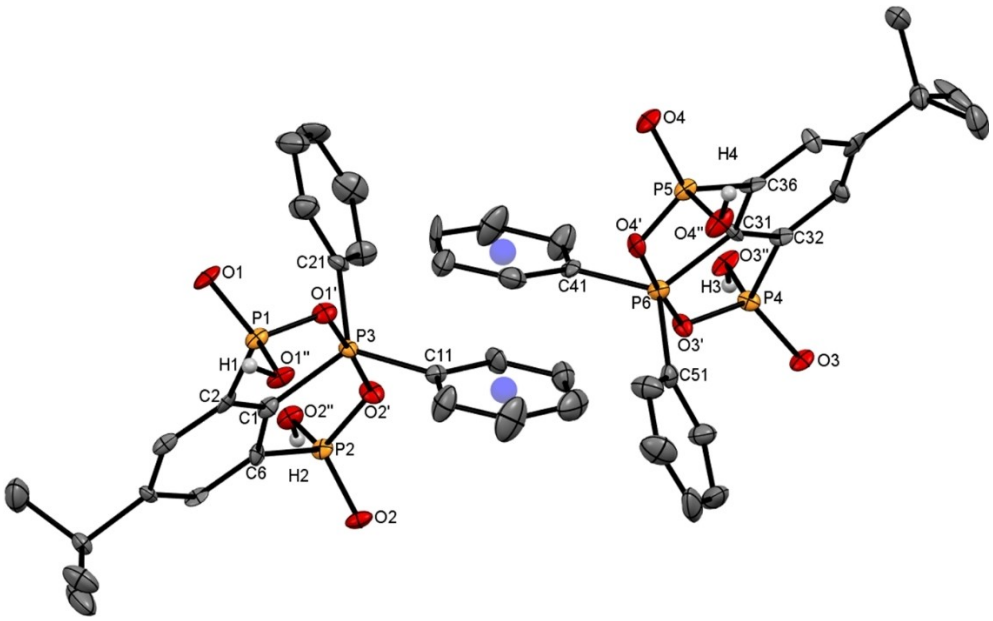

Figure 7. Molecular structure and atom numbering scheme showing the two independent molecules of the aryldiphenyldioxaphosphorane diastereomer **7a**·2$CHCl_3$ existing as pairs of enantiomers (*RR*/*SS*). Displacement ellipsoids are drawn at 30 % probability level. The $CHCl_3$ solvate molecules are omitted for clarity. With exception of the OH protons, hydrogen atoms were omitted for clarity. The blue dots indicate the centroids of the phenyl substituents with a distance of 4.256(1) Å. Table S2 in the Supporting Information contains selected interatomic distances and angles.

respectively, are considerably longer than the distances to the oxygen atoms bound to P1, P2, P4, and P5. This reflects their axial position in the trigonal bipyramid and follows Bents polarity rule[28] according to which axial bonds are longer than equatorial ones. The phenyl substituents containing C11 and C41 are face-to-face to each other with a [C11–C16]-centroid to [C41–C46]-centroid distance of 4.256(1) Å, a distance too large to support a π-stacking interaction.[29]

Intermolecular O1′′-H1···O2A, O2′′-H2···O1A, O3′′-H3···O4A and O4′′-H4···O3A hydrogen bridges with O···O distances of 2.511(7), 2.495(6), 2.459(7), and 2.509(5) Å, respectively, give two strands of one-dimensional polymers involving eight-membered $P_2O_4H_2$ rings (Figure 8, Table 2). A Graph Set analysis of this pattern gives $N_1\left[C_1^2(8)\middle|R_2^2(8)\right]$. In addition, there are O1···H3LA and O3···H4LA contacts at distances of 2.478(1) and 2.368(1) Å, respectively. These are shorter than the sum of the van der Waals radii[27] of oxygen (1.52 Å) and hydrogen (1.10 Å).

The aryldiphenyldioxaphosphorane diastereomer isopropanol solvate **7b**·*i*-PrOH crystallized from its solution in a solvent mixture consisting of CH_2Cl_2 and diethyl ether in the orthorhombic space group $P2_12_12_1$ with four molecules in the unit cell (Table S1 in Supporting Information). Figure 9 shows its molecular structure and Table S3 in the Supporting Information contains selected interatomic distances and angles. The single crystal actually investigated by X-ray diffraction analysis contained only the *SR* enantiomer indicating spontaneous racemate separation. Rather likely, other crystals of the bulk material contained the *RS* enantiomer. However, this was not confirmed by X-ray diffraction of different crystals. The intramolecular interatomic distances and angles are rather close to those observed for **7a**·2$CHCl_3$ and deserve no further discussion. However, in both **7a**·2$CHCl_3$ and **7b**·*i*-PrOH the axial P-O distances differ slightly [1.756(4)/1.789(4) Å and 1.762(4)/1.801(4) Å in **7a**·2$CHCl_3$; 1.791(2)/1.776(2) Å in **7b**·*i*-PrOH].

Table 2. Interatomic distances (Å) and angles (°) for the hydrogen bridges in **7a**·2$CHCl_3$.

D-H···A	d(D-H)	d(H···A)	d(D···A)	(DHA)
O1′′-H1···O2A[i]	0.75(2)	1.89(5)	2.511(6)	139(7)
O2′′-H2···O1A[ii]	0.78(2)	1.72(2)	2.495(6)	174(8)
O3′′-H3···O4A[ii]	0.80(2)	1.66(3)	2.459(7)	173(7)
O4′′-H4···O3A[i]	0.81(2)	1.75(4)	2.509(5)	156(8)

Symmetry transformations used to generate equivalent atoms: [i] x, y+1, z ; [ii] x, y-1, z.

A search in the Cambridge Crystallographic Database reveals ten crystal structures[30] of triorganodioxaphosphoranes in which both oxygen atoms occupy axial positions and show P-O distances ranging between 1.79(1)[30a] and 1.71(1) Å.[30a] The axial O-P-O angles vary between 178.40(7) [30d] and 165.8(6)°.[30a] The structural data for **7a**·2$CHCl_3$ and **7b**·*i*-PrOH are close to these values.

A major difference in the crystal structure of the aryldiphenyldioxaphosphorane **7b**·*i*-PrOH as compared to the corresponding phosphorane diastereomer **7a**·2$CHCl_3$ is the way the crystallographic identical molecules are linked by hydrogen bridges. There are O1′′-H1′′···O2 A, O2′′-H2′′···O1LA, and O1-H1L···O1 hydrogen bridges with O···O distances of 2.550(3), 2.480(4), and 2.639(4) Å, respectively, involving both the P-O*H* and the *i*-PrO*H* protons and forming ten-membered $P_2O_5H_3$ rings giving a one-dimensional polymer (Figure 10, Table 3),

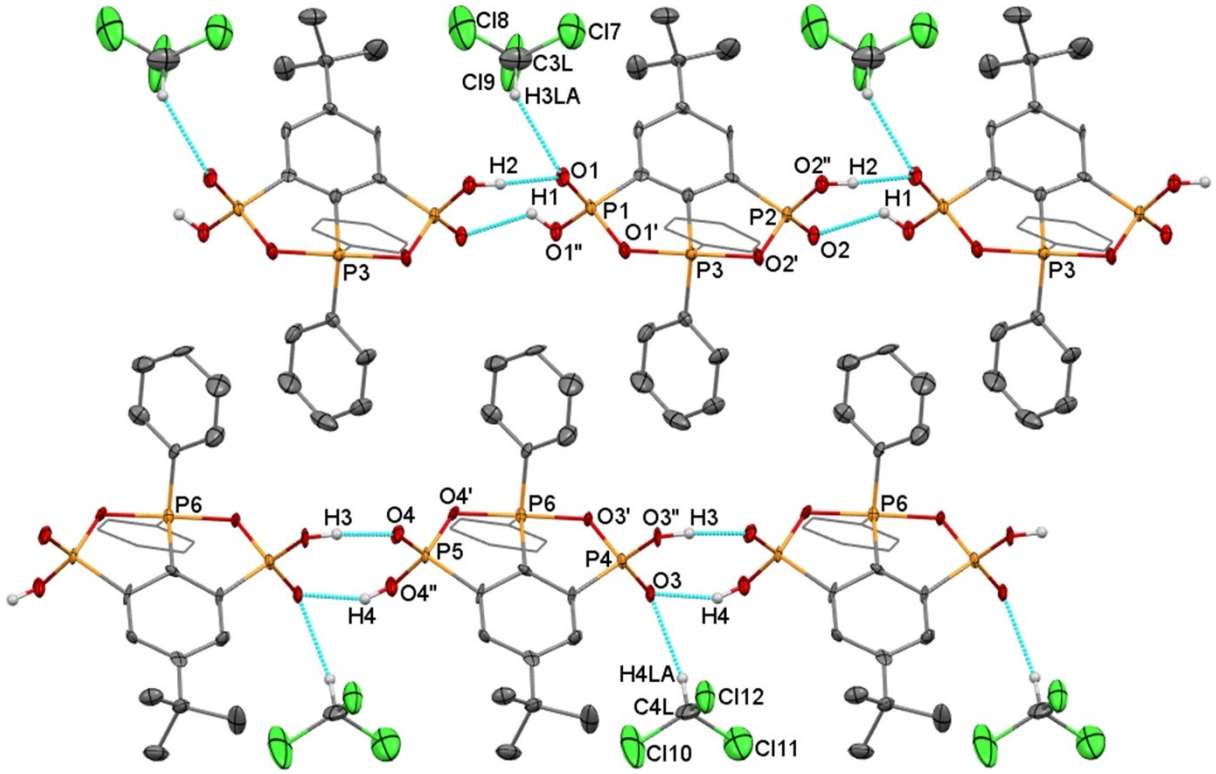

Figure 8. Portion of the crystal structure of **7a**·2CHCl$_3$ showing the one-dimensional chain generated by hydrogen bridges. With exception of the OH protons, the hydrogen atoms were omitted for clarity. Displacement ellipsoids are drawn at 30% probability level.

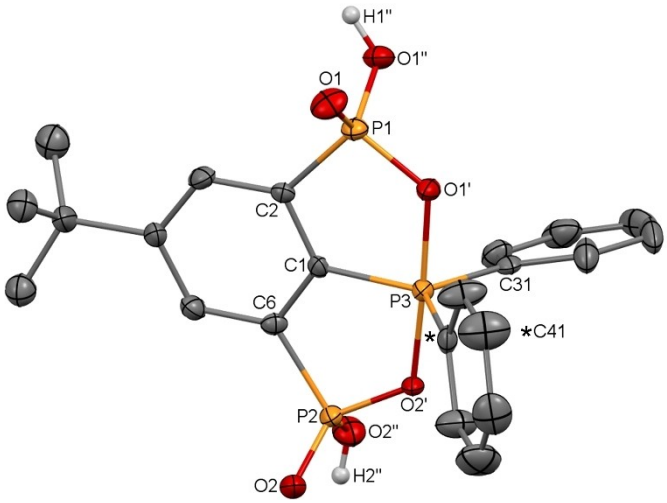

Figure 9. Molecular structure and atom numbering scheme of **7b**·*i*-PrOH (*SR* enantiomer). Displacement ellipsoids are drawn at 30% probability level. The *i*-PrOH molecule and hydrogen atoms but those belonging to the OH groups were omitted for clarity.

Table 3. Interatomic distances (Å) and angles (°) for the hydrogen bridges in **7b**·*i*-PrOH (*SR*).

D-H···A	d(D-H)	d(H···A)	d(D···A)	(DHA)
O1″-H1″···O2A[i]	0.83(4)	1.73(4)	2.550(3)	168(4)
O2″-H2″···O1LA[ii]	0.70(4)	1.80(4)	2.480(4)	164(5)
O1L-H1L···O1	0.73(5)	1.91(5)	2.639(4)	177(6)

Symmetry transformations used to generate equivalent atoms: [i] -x+3/2, -y+1, z-$^1/_2$; [ii] -x+3/2, -y+1, z+$^1/_2$.

with a Graph Set analysis[31] giving $N_1[C_1^1(8)|R_3^3(10)]$. The remarkable high melting point of 387 °C indicates the high stability of these hydrogen bonds.

The structures of the aryldiphenyldioxaphosphoranes diastereomers **7a**·2CHCl$_3$ and **7b**·*i*-PrOH can be compared to those of related isoelectronic species **I/I′**, **III/III′/III″**, diastereomers (*RR/SS*)-**V** (**Va**) and (*RS/SR*)-**V** (**Vb**), and the related hypothetical benzoxaphosphaphosphole cation **II/II′** (Scheme 4).

By considering the covalent radii[27] of phosphorus, silicon and oxygen atoms (1.10, 1.18, and 0.73 Å, respectively), the P-O$_{ax}$ [1.756(4)-1.801(4) Å] and P*-O(H)/P*-OP [1.516(5)-1.573(5) Å] distances determined for **7a**·2CHCl$_3$ and **7b**·*i*-PrOH are shorter than the sum of the covalent radii (1.83 Å) of the atoms involved. One reason for this could be tentatively ascribed to a considerable ionic character of the bonds inducing electrostatic attraction. On the other hand, the Si-O distances of 1.9225(14) and 1.9312(14) Å reported for the intramolecularly P=O→Si coordinated triorganosiliconium cation **III**[3] are rather close to the sum of the covalent radii (1.91 Å) of silicon and oxygen atoms. Apparently, the bonding situation is reflected to some extent by participation of the canonical formula **III″**. In case of the benzoxaphosphasilole,[2] the canonical formula **IV** reflects best the reality with rather short Si-OP* [1.715(3) Å] and long Si←O=P [2.672(3) Å] interatomic distances (Scheme 4).

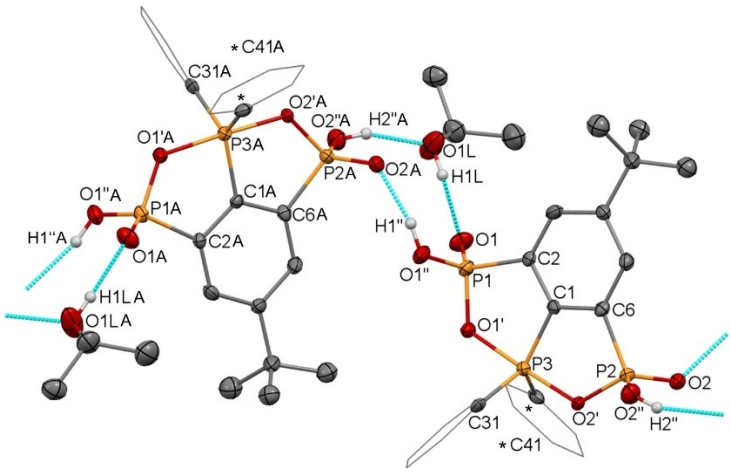

Figure 10. Portion of the crystal structure of phosphorane **7b**·*i*-PrOH (*SR* enantiomer) showing the one-dimensional chain generated by hydrogen bridges. With the exception of the OH protons, the hydrogen atoms were omitted for clarity. Displacement ellipsoids are drawn at 30% probability level.

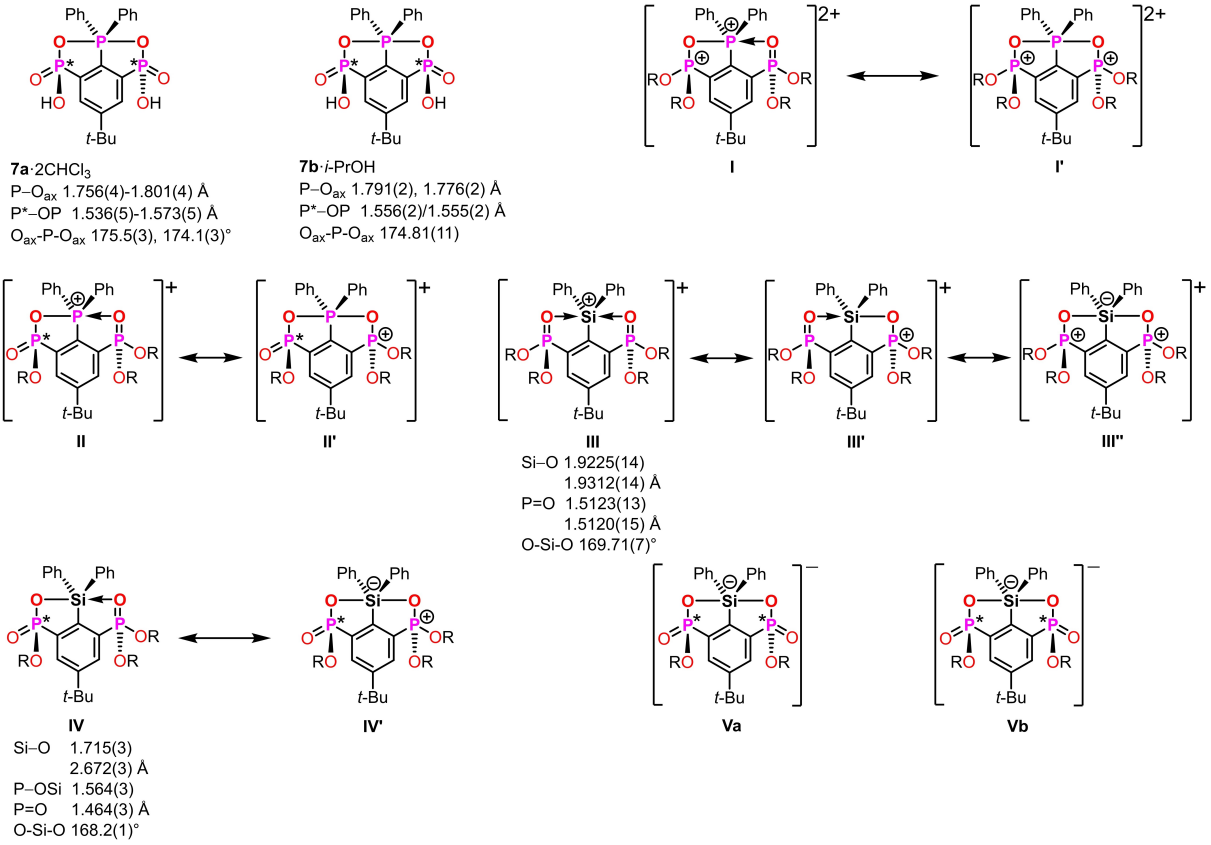

Scheme 4. Comparison of selected interatomic distances and angles for the aryldiphenyldioxaphosphoranes diastereomers **7a**·2CHCl$_3$ and **7b**·*i*-PrOH with related known isoelectronic compounds **III/III′/III″** and **IV/IV′**, so far unknown isoelectronic species **I/I′**, diastereomers **Va** and **Vb**, and the hypothetical benzoxaphosphaphosphole cation **II/II′**, which are related to the other non-isoelectronic species.

Theoretical calculations

In order to get an insight into the electronic structure and properties of the aryldiphenylphosphane chalcogenides **1**–**3** and their derivatives, a computational investigation was carried out at the density functional theory (DFT)[32] level. A preliminary validation of the computational setup was carried out on the aryldiphenylphosphane **6** by testing different combinations of functionals and basis sets (Supporting Information, Table S4), eventually leading to the choice of the hybrid mPW1PW functional[33] in combination with Ahlrichs triple-ζ basis sets (BSs) in Weigend's formulation (def2-TZVP),[34] featuring Relativ-

istic Effective Core Potentials (RECPs)[35,36] on the heavier iodine species (Supporting Information, Tables S5–S24). Metric parameters optimized for compounds **1**, **2**, **5b**, **6**, **7a**, and **7b** in the gas phase show a very good agreement with structural data (Supporting Information, Table S25), interatomic distances and angles differing in most cases by less than 0.03 Å and 6°, respectively. The only exceptions are P-O distances involving oxygen atoms that participate in hydrogen bonds in the solid state (see below for the aryldiphenyldioxaphosphoranes **7a** and **7b**).

In the aryldiphenylphosphane chalcogenides **1**–**3** (Figure S128, Tables S5-S7), optimized in the C_s point group, NBO calculations do not provide evidence of any O→P donor-acceptor interaction, the relevant Wiberg bond indexes being as low as 0.006. Accordingly, a second order perturbation theory (SOPT) analysis of the Fock matrix in the NBO basis does not show any O1/O2→P3 charge-transfer (numbering scheme as in Figure S128). This notwithstanding, the optimized O1/O2-P3 distances (3.223, 3.267, and 3.273 Å for **1**, **2**, and **3**, respectively), are calculated to be shorter than the sum of van der Waals radii (3.47 Å) in agreement with the single crystal X-ray diffraction analysis. On the other hand, the P3 atom in the aryldiphenylphosphane chalcogenides **1**–**3** bears a significant positive natural charge[37] (Q_P = 1.966, 1.368, and 1.280 |e| for E = O (**1**), S (**2**) and Se (**3**), respectively; Table S26), and a strong polarization of the P-E bond is observed, decreasing on passing from E = O to E = Se ($|\Delta Q_{P\text{-}E}|$ = 3.031, 1.928, and 1.754 |e|, for **1**, **2** and **3**, respectively). The positive charge Q_P along with the strongly negative charge on the atom O1/O2 (−1.080 |e|, Table S26) support an electrostatic interaction $O^{\delta-}\cdots P^{\delta+}$ decreasing from the aryldiphenylphosphane oxide **1** to the aryldiphenylphosphane selenide **3**, reflected in the order of O1/O2···P3 distance optimized for **1**, **2**, and **3**.

The natural charge distribution calculated for the aryldiphenylphosphane chalcogenides **1**–**3**, along with the localization of the LUMO + 2 Kohn-Sham (KS) molecular orbital (MO) on P3 (Figure 11 for **2**), nicely account for the reduction process leading from the aryldiphenylphosphane sulfide **2** to the aryldiphenylphosphane **6** (Scheme 3; Q_P = 0.860 |e|, Table S26) and the partial hydrolysis of the aryldiphenylphosphane oxide **1** affording the partially hydrolysed aryldiphenylphosphane oxide **4** (Scheme 3) observed experimentally. Consistently with the experimental data, upon reduction of the aryldiphenylphosphane sulfide **2** to the corresponding aryldiphenylphosphane **6**, a rotation of the phenyl substituents occurs, and the two rings are arranged in a propeller-like fashion, featuring calculated torsions of 108.69 and 59.33°, respectively, with respect to the plane of the central aromatic ring (Figure S128, Table S10). As expected, the KS-HOMO of **6** is mainly built up of the lone pair of electrons on the P3 atom featuring a trigonal pyramidal geometry (Figure 11).

In case of the benzoxaphosphaphosphole sulfide derivative **5**, the two possible diastereomers (*RR*/*SS*)-**5** (**5a**) and (*RS*/*SR*)-**5** (**5b**) were optimized (Supporting Information, Tables S8-S9, Figure S129). The two diastereomers show very similar metric parameters and charge distribution (Supporting Information, Table S26, Table S25), and total electronic energies differing by less than 1.0 kcal/mol, thus suggesting that the formation of diastereomer **5a** cannot be excluded on thermodynamic grounds, and that its missed isolation could be attributed to experimental purification steps after the synthesis, as suggested above.

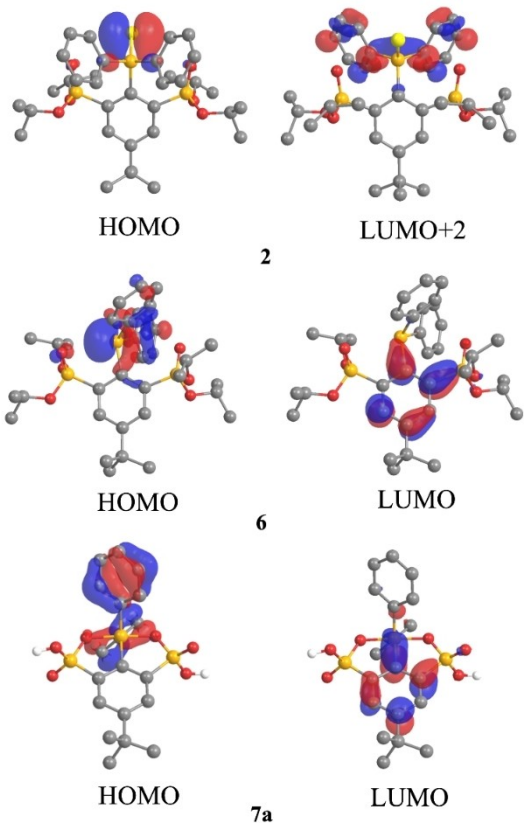

Figure 11. Isosurfaces of selected Kohn–Sham frontier molecular orbitals calculated at the optimized geometry in the gas phase for the aryldiphenylphosphane sulfide **2**, the aryldiphenylphosphane **6**, and the aryldiphenyldioxaphosphorane **7a** at DFT level (mPW1PW/def2-TZVP). Cutoff value = 0.05 |e|; only the hydrogen atoms of the hydroxyl groups are shown for clarity.

DFT calculations have been exploited to postulate a possible mechanism for the reaction leading from the aryldiphenylphosphane **6** to the aryldiphenyldioxaphosphorane **7** (Scheme 3). It is well known that a triarylphosphane can act as Lewis base towards diiodine, I_2, leading to 1:1 charge-transfer (CT) adducts featuring a roughly linear P-I-I moiety.[38] The same type of CT adducts with dibromine, Br_2, has been reported occasionally.[39] It could be hypothesized that the formation of a phosphane dihalogen CT adduct **6**·X_2 [X = Br (**8**) and I (**9**)] may be the first step in the dihalogen (X_2) oxidation leading from the aryldiphenylphosphane **6** to the aryldiphenyldioxaphosphorane **7** (Scheme 5). The CT-adducts **8** and **9** were successfully optimized (Supporting Information, Figure S130, Tables S15–S16), showing a considerable charge separation in the P-X-X moiety (Table S26), the P3 atom bearing a positive natural charge (Q_P = 1.323 and 1.145 |e| in **8** and **9**, respectively), while the terminal halogen atom is negatively charged (Q_{X2} = −0.574 and −0.392 |e| in **8** and **9**, respectively) and the central one is

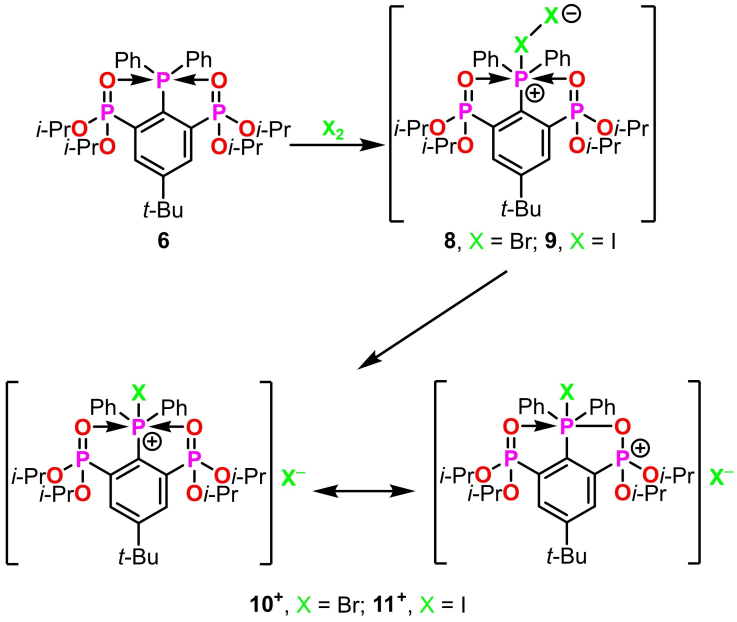

Scheme 5. Proposed mechanism for the initial steps in the formation of **7** by dihalogen X_2 oxidation of compound **6** through intermediates **8**, **9**, $\mathbf{10}^+$ and $\mathbf{11}^+$ (X = Br, I).

almost neutral (Q_{XI} = −0.066 and −0.005 |e| in **8** and **9**, respectively). This charge distribution closely resembles that calculated for 1:1 CT "spoke" adducts of chalcogenone donors **L**=E (**L** = organic framework, E = S, Se), with dihalogens, interhalogens and pseudohalogens[40] for which a role of the hypothetical cation $[\mathbf{L}{=}\mathrm{E}{\cdot}\mathrm{X}]^+$ was postulated in the formation of oxidized products.[41] Indeed, the charge distribution on this model cation was a useful parameter in understanding the possible reaction products, including, in addition to "spoke" CT adducts, neutral "T-shaped" hypercoordinate chalcogen species **L** = E(X)X, dications $[\mathbf{L}\text{-}\mathrm{E}]_2^{2+}$ containing a single chalcogen-chalcogen bond and oxidized cations $[\mathbf{L}\text{-}\mathrm{X}]^+$, formally derived from a carbon-chalcogen double-bond cleavage promoted by the dihalogen or the interhalogen.[41] Prompted by these results and the large charge separation between the two halogen atoms X in the CT-adducts **8** and **9**, indicating a partially ionic nature $[\mathbf{6}{\cdot}\mathrm{X}]^+\mathrm{X}^-$[40] increasing on passing from **8** to **9**, DFT calculations were extended to the hypothetical intermediates $\mathbf{10}^+$ and $\mathbf{11}^+$ (Scheme 5, Figure S130, Tables S17-S18). As expected, in $\mathbf{10}^+$ and $\mathbf{11}^+$ an increase by about 0.2-0.3 |e| in the positive charge of P3 is calculated with respect to **8** and **9** (Table S26). Moreover, in $\mathbf{10}^+$ and $\mathbf{11}^+$ the KS-LUMO, antibonding with respect to the P-X bond (Figure 12), is largely localized on the phosphorus atom. Therefore, the charge distribution on the hypothetical model cation $\mathbf{10}^+/\mathbf{11}^+$ supports a strongly electrophilic character for the halogen-coordinating P-atom in the halophosphonium species $\mathbf{10}^+/\mathbf{11}^+$, thus accounting for the formation of the aryldiphenyldioxaphosphorane **7** (Scheme 5). The subsequent steps leading to **7** are likely analogous to the mechanism reported for the formation of the benzoxaphospha(semi)metalloles[3] and involve nucleophilic attack of the halide anion at the OC carbon centre followed by elimination of *iso*-propyl halide and cyclization. So far, we have no explanation for the fast hydrolysis under mild conditions of the two remaining *iso*-propoxide substituents during the crystallization process under non-inert conditions.

In the case of compound **7**, the two diastereomers **7a** and **7b** (Tables S11-S12 and Figure 13), as expected, differ by less than 1.0 kcal/mol, in the total electronic energies. **7a** and **7b** were also optimized in $CHCl_3$ solution (thus simulating the conditions of the crystallization of $\mathbf{7a}{\cdot}2CHCl_3$), the solvation been implicitly accounted for at the IEF-PCM level[42] (Tables S13–S14). The optimized geometries in $CHCl_3$ were calculated to be very close to those in the gas phase, with only minor differences in bond distances and angles (less than 0.01 Å and 1°, respectively; Table S25). As mentioned above, in the case of **7a** and **7b** a not negligible difference can be observed between the optimized P-O bond lengths at the phosphonic sites and the corresponding structural data (Tables S2-S3). In particular, in the case of diastereomer **7a** the P=O and P-OH distances at the optimized geometry are underestimated by about 0.08 and overestimated by 0.03 Å, respectively, when compared to structural data. This is most likely attributable to hydrogen bonding interactions between neighbouring molecule units involving the phosphonic oxygen atoms. Analogously, the overestimation of the P-OH bond lengths in diastereomer **7b** by about 0.07 Å is possibly due to the involvement of the P*OH* substituent in hydrogen bonds with co-crystallized isopropanol molecules observed in the solid-state structure (see above). In agreement with experimental data, the metric parameters of the two diastereomers **7a** and **7b** were calculated to be strikingly similar to each other (Table S25), with P=O, P-OH and P-OP distances of 1.466 (1.469 in $CHCl_3$), 1.597 (1.594 in $CHCl_3$), and 1.564 (1.563 in $CHCl_3$) Å,

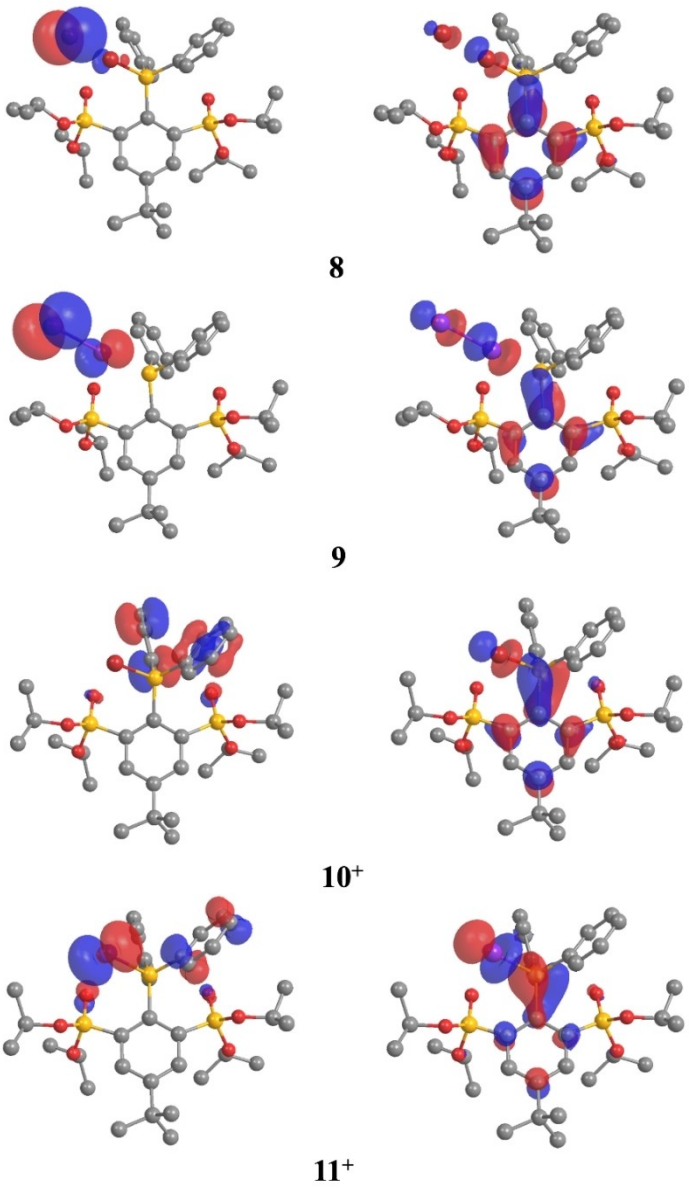

Figure 12. Isosurfaces of Kohn–Sham HOMOs (left) and LUMOs (right) calculated at the optimized geometry for **8**, **9**, **10**$^+$ and **11**$^+$ in the gas phase at DFT level (mPW1PW/def2-TZVP). Cut-off value = 0.05 |e|; hydrogen atoms were omitted for clarity.

respectively. Accordingly, the charge distribution is similar in both **7a** and **7b**, showing an increase ΔQ_P in the positive charge of the atom P3 of about 1.0 |e| upon oxidation of the aryldiphenylphosphane **6** to the corresponding aryldiphenyl-dioxaphosphorane **7**, and a charge of −1.077 |e| on the oxygen atom of the P-O-P moiety (Table S26).

In order to further rationalize the nature of the bonding in these systems and in their Si-analogues discussed above, compounds **I**–**V** (Scheme 4) were optimized at the same level of theory (Table 4, S19-S24, S27-S28, Figure 13).

The calculated data collected in Table 4 allow for a comparison of selected structural parameters for the pentacoordinated compounds **I**/**I**′,**Va**/**Vb**, **7a** and **7b**. All these compounds have in common a trigonal bipyramidal structure in which three carbon atoms (the C_{ipso} carbon atoms from the three aryl substituents) bind the central element Y (Y = P3 or Si1) in equatorial and two oxygen atoms in axial positions. The equatorial C-Y-C angles vary between 114.98 (C31-Si1-C41, **Va**) and 123.55° (C1-Si1-C31, **Va**), and the axial O-Y-O angles between 169.80 (**IV**/**IV**′) and 176.57° (**7a**), indicating relatively small deviations from the ideal trigonal-bipyramidal geometry. The P1-C2-C1 and P2-C6-C1 angles vary between 109.93 (**III**/**III**′/**III**″) and 115.66° (**II**/**II**′), while the Y-C1-C2 and Y-C1-C6 angles range from 112.79 (**II**/**II**′) to 128.03° (**II**/**II**′). The comparison of the species **7a**/**7b** with the isoelectronic dication **I**/**I**′ reveals the P3-O1′ and P3-O2′ distances being slightly longer for **I**/**I**′ but almost equal within the compounds. This suggest the mesomeric formula of type **I**′ to dominate in both compounds. The

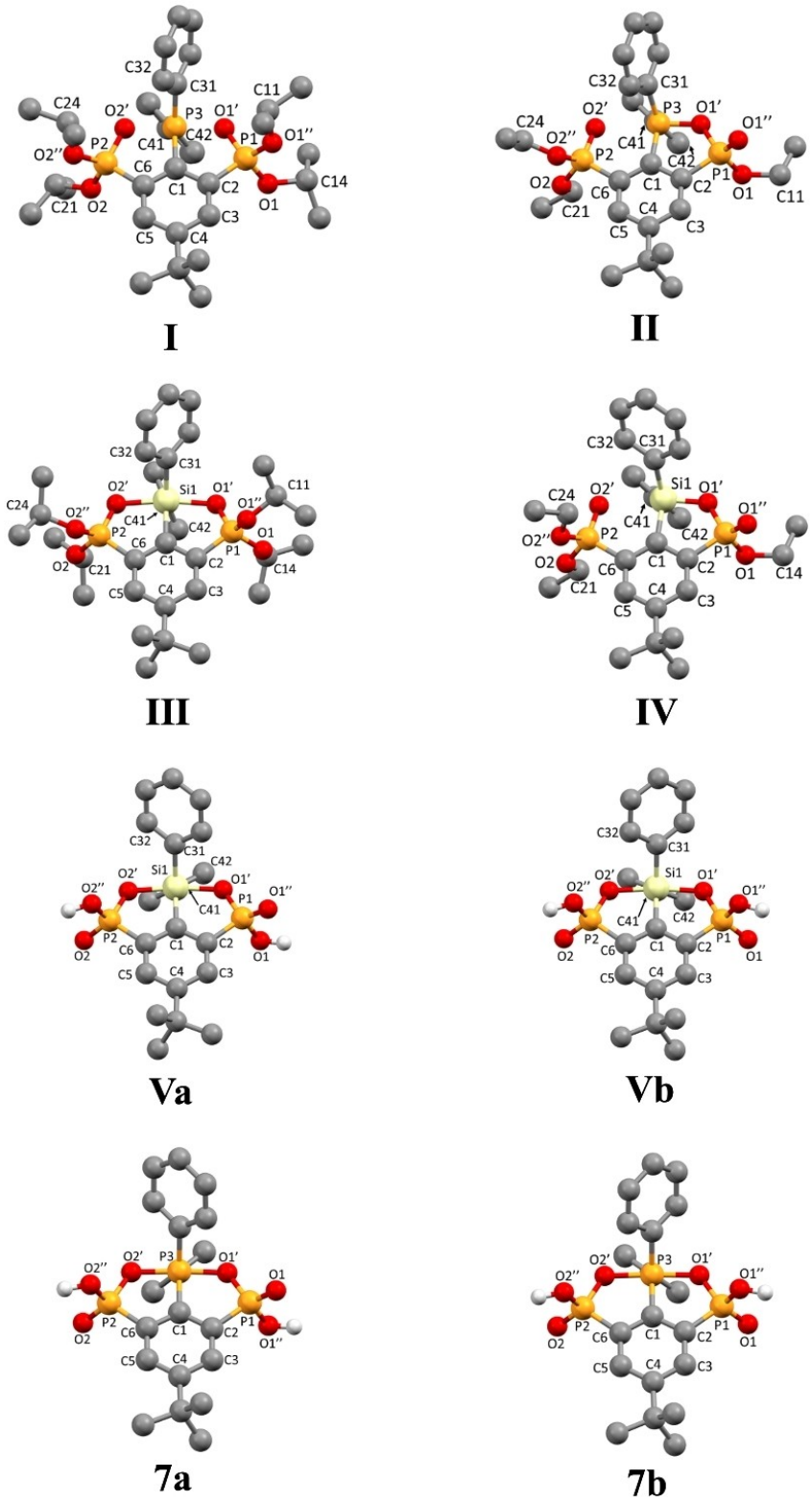

Figure 13. Molecular drawings and atom labelling scheme of **7a**/**7b**, **I**–**IV** and **Va**/**Vb** at the DFT-optimized geometry in the gas phase (mPW1PW/def2-TZVP; hydrogen atoms omitted for clarity).

same picture holds for the monocationic silicon species **III**/**III**′/**III**″ showing almost equal Si1-O1′ and Si1-O2′ distances (as established by single crystal X-ray diffraction analysis). On the other hand, the structurally related monocation **II**/**II**′ shows rather different P3-O1′ and P3-O2′ distances, suggesting that the mesomeric formula **II** is dominant. This compound finds its

Table 4. Selected interatomic distances (Å) and angles (°) for compounds **I**–**V** and **7a**/**7b** at the optimized geometry in the gas phase (mPW1PW/def2-TZVP; labelling schemes as in Figure 13). The numbers decorated with ′ or ″ refer to mesomeric structures/canonical formulas.

	I/I′ Y<=>P3	**II/II′** Y=P3	**III/III′/III″** Y=Si1	**IV/IV′** Y=Si1	**Va** Y=Si1	**Vb** Y=Si1	**7a** Y=P3	**7b** Y=P3
P1-O1′	1.539	1.623	1.513	1.570	1.539	1.538	1.564	1.564
P1-O1″	1.540	1.569	1.551	1.593	1.618	1.619	1.597	1.597
P1-O1	1.536	1.455	1.561	1.467	1.476	1.476	1.466	1.466
P3-O2′	1.539	1.484	1.513	1.480	1.538	1.539	1.564	1.565
P3-O2″	1.540	1.562	1.552	1.576	1.618	1.624	1.597	1.604
P3-O2	1.535	1.571	1.560	1.576	1.476	1.474	1.466	1.463
P1-C2	1.776	1.793	1.776	1.799	1.799	1.799	1.791	1.791
P3-C6	1.776	1.781	1.776	1.781	1.800	1.798	1.791	1.791
Y-C1	1.816	1.812	1.900	1.898	1.895	1.897	1.816	1.816
Y-C31	1.797	1.783	1.868	1.878	1.903	1.903	1.818	1.818
Y-C41	1.796	1.790	1.870	1.874	1.903	1.904	1.818	1.818
Y-O1′	1.833	1.626	1.947	1.721	1.866	1.868	1.772	1.774
Y-O2′	1.841	2.450	1.937	2.492	1.868	1.869	1.773	1.774
C1-Y-C31	120.07	117.05	122.19	117.99	122.38	123.55	121.80	123.35
C1-Y-C41	121.91	119.63	119.17	117.15	122.34	121.47	121.81	120.55
C31-Y-C41	118.02	115.80	118.64	119.03	115.27	114.98	116.39	116.09
Y-O1′-P1	121.51	121.76	118.76	122.17	123.00	123.20	123.57	123.73
P1-C2-C1	111.02	114.45	109.93	113.49	111.25	111.29	111.56	111.61
Y-C1-C2	120.29	112.79	121.38	113.84	120.36	120.31	119.64	119.63
Y-O2′-P3	120.00	110.79	119.91	111.31	123.85	123.04	123.69	123.49
P3-C6-C1	110.50	115.66	110.39	114.91	111.26	111.30	111.55	111.65
Y-C1-C6	120.43	128.03	121.10	128.62	120.32	120.40	119.68	119.66
O1′-Y-O2′	175.41	175.05	170.96	169.80	171.82	171.60	176.57	176.21
P1-C2-C1-Y	1.94	1.89	2.08	0.88	1.33	1.21	2.22	0.35
P3-C6-C1-Y	2.59	0.19	1.21	0.74	1.11	1.94	2.08	0.80

silicon analogue in the neutral species **IV/IV′**, with rather different Si1-O1′ and Si1-O2′ distances (as also established by single crystal X-ray diffraction analysis).

Finally, an analysis of isoelectronic couples **7a**/**Va** and **7b**/**Vb** shows that the Y-O1′/Y-O2′ interatomic distances (Y = P3 or Si1) optimized in the gas phase are shorter by an average of 0.057 Å for compounds **7a** and **7b** (Y = P3) and 0.042 Å for **Va** and **Vb** (Y = Si1) than the sum of the covalent radii of the atoms involved, as a consequence of the trigonal-bipyramid geometry at the Y atoms, corresponding to average Wiberg bond indexes of 0.496 and 0.373, respectively. A SOPT analysis allows to evaluate the energy of the bonds between the O1′/O2′ atoms and Y atom (Y = P3 or Si1; numbering scheme as in Figure 13) in about 150 and 227 kcal/mol for **7a**/**7b** and **Va**/**Vb**, respectively. On the other hand, the hypothetical benzoxaphosphaphosphole dication **I** shows average calculated P3-O1′/P3-O2′ distances longer than those of **7a**/**7b** by about 0.064 Å, and roughly corresponding to the sum of oxygen and phosphorus covalent radii, in analogy with its isoelectronic silicon analogue **III**. This suggests that Y-O interatomic distances largely depend on the molecular charge of the compound, rather than on the identity of Y.

Conclusions

We have reported a variety of P^{III} and P^{V} compounds containing the potentially intramolecularly O,C,O-coordinating pincer-type ligand [5-*t*-Bu-1,3-{(P(O)(O-*i*-Pr)$_2$}$_2$C$_6$H$_2$]$^-$. In successive oxidation and hydrolysis reactions, the latter was, for the first time, involved in a double cyclization giving diastereomeric aryldiphenyldioxaphosphoranes. Based on DFT calculations, a possible mechanism for the oxidation key process with I_2 or Br_2 of the aryldiphenylphosphane has been proposed. The analysis on the structural features of aryldiphenyldioxaphosphoranes were extended to the Si^{IV} isoelectronic analogue and related hypercoordinate P^{V} and Si^{IV} compounds. Our results suggest that differences in the metric parameters depend on the identity of the central hypercoordinate atom in its higher oxidation state. On the other hand, the double cyclization resulting in the trigonal bipyramidal geometry at the P^{V} and Si^{IV} centres relies on the symmetry of the O,C,O-coordinating pincer-type ligand.

The compounds **1**–**3** and **6** containing both hard and soft donor sites hold potential as chelate ligands towards transition metals. A detailed report on this behaviour will be a subject of a forthcoming paper.

A search in the Cambridge Crystallographic Database showed that the triorganodioxaphosphoranes **VII**–**X** (Scheme 6) are not known. They are related to the aryldiphenyldioxaphosphorane reported herein and might be interesting target molecules to be synthesized in the future.

Experimental Section

For the syntheses and complete characterization of the compounds **1**–**7**, the crystallography, and the DFT calculations see the Supporting Information. Deposition Numbers 2160847 (for **1**), 2160848 (for **2**), 2160849 (for **3**), 2160850 (for **4**), 2160851 (for **5**), 2160852 (for **6**), 2160853 (for **7b**·*i*-PrOH), and 2160854 (for **7a**·2CHCl$_3$) contain the supplementary crystallographic data for this paper. These data are provided free of charge by the joint Cambridge Crystallographic Data Centre and Fachinformationszentrum Karlsruhe Access Structures service.

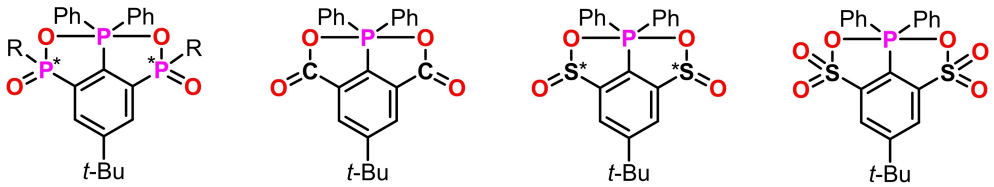

Scheme 6. Triorganodioxaphosphoranes which are related to the compounds reported in this manuscript but which are hitherto unknown.

Acknowledgements

The authors kindly acknowledge CINECA for the computational resources on the Galileo 100 supercomputer accessed within the ISCRA project QMPhosp (code HP10CHQL9T). KJ thanks the PhD students Justin Wieland and Hendrik Busen (research team Prof. A. Steffen at TU Dortmund) for processing some NMR spectra. We thank the anonymous reviewers for careful examination of the manuscript and helpful comments. Open Access funding enabled and organized by Projekt DEAL.

Conflict of Interest

The authors declare no conflict of interest.

Data Availability Statement

The data that support the findings of this study are available in the supplementary material of this article.

Keywords: DFT calculations · NMR spectroscopy · phosphorus triorganodioxaphosphorane · X-ray diffraction

[1] K. Peveling, M. Schürmann, K. Jurkschat, *Main Group Met. Chem.* **2001**, *24*, 251–252.
[2] K. Peveling, M. Schürmann, R. Ludwig, K. Jurkschat, *Organometallics* **2001**, *20*, 4654–4663.
[3] K. Peveling, M. Henn, C. Löw, M. Mehring, M. Schürmann, B. Costisella, K. Jurkschat, *Organometallics* **2004**, *23*, 1501–1508.
[4] K. Peveling, K. Dannappel, M. Schürmann, B. Costisella, K. Jurkschat, *Organometallics* **2006**, *25*, 368–374.
[5] K. Dannappel, M. Schürmann, B. Costisella, K. Jurkschat, *Organometallics* **2005**, *24*, 1031–1034.
[6] K. Dannappel, R. Nienhaus, M. Schürmann, B. Costisella, K. Jurkschat, *Z. Anorg. Allg. Chem.* **2009**, *635*, 2126–2134.
[7] M. Mehring, M. Schürmann, K. Jurkschat, *Organometallics* **1998**, *17*, 1227–1236.
[8] M. Mehring, C. Löw, M. Schürmann, K. Jurkschat, *Eur. J. Inorg. Chem.* **1999**, 887–898.
[9] M. Mehring, C. Löw, M. Schürmann, F. Uhlig, K. Jurkschat, B. Mahieu, *Organometallics* **2000**, *19*, 4613–4623.
[10] M. Mehring, I. Vrasidas, D. Horn, M. Schürmann, K. Jurkschat, *Organometallics* **2001**, *20*, 4647–4653.
[11] M. Henn, M. Schürmann, B. Mahieu, P. Zanello, A. Cinquantini, K. Jurkschat, *J. Organomet. Chem.* **2006**, *691*, 1560–1572.
[12] V. Deáky, M. Schürmann, K. Jurkschat, *Z. Anorg. Allg. Chem.* **2009**, *635*, 1380–1383.
[13] M. Henn, V. Deáky, St. Krabbe, M. Schürmann, M. H. Prosenc, S. Herres-Pawlis, B. Mahieu, K. Jurkschat, *Z. Anorg. Allg. Chem.* **2011**, 637, 211–223.
[14] M. Wagner, K. Dorogov, M. Schürmann, K. Jurkschat, *Dalton Trans.* **2011**, *40*, 8839–8848.
[15] M. Wagner, C. Dietz, S. Krabbe, S. G. Koller, C. Strohmann, K. Jurkschat, *Inorg. Chem.* **2012**, *51*, 6851–6859.
[16] M. Wagner, M. Henn, C. Dietz, M. Schürmann, M. H. Prosenc, K. Jurkschat, *Organometallics* **2013**, *32*, 2406–2415.
[17] M. Wagner, V. Deáky, C. Dietz, J. Martincová, B. Mahieu, R. Jambor, S. Herres-Pawlis, K. Jurkschat, *Chem. Eur. J.* **2013**, *19*, 6695–6708.
[18] M. Wagner, T. Zöller, W. Hiller, M. H. Prosenc, K. Jurkschat, *Chem. Eur. J.* **2013**, *19*, 9463–9467.
[19] M. Wagner, T. Zöller, C. Dietz, K. Jurkschat, *Main Group Met. Chem.* **2015**, 38, 169–173.
[20] M. Wagner, M. Lutter, C. Dietz, M. H. Prosenc, K. Jurkschat, *Eur. J. Inorg. Chem.* **2015**, 2152–2158.
[21] K. Peveling, M. Schürmann, K. Jurkschat, *Z. Anorg. Allg. Chem.* **2002**, *628*, 2435–2442.
[22] K. Jurkschat, K. Peveling, M. Schürmann, *Eur. J. Inorg. Chem.* **2003**, 3563–3571.
[23] K. Peveling, M. Schürmann, S. Herres-Pawlis, C. Silvestru, K. Jurkschat, *Organometallics* **2011**, *30*, 5181–5187.
[24] T. Řezníček, L. Dostál, A. Růžička, R. Jirásko, R. Jambor, *Inorg. Chim. Acta* **2010**, *363*, 3302–3307.
[25] L. Dostál, R. Jambor, A. Růžička, R. Jirásko, J. Holeček, F. De Proft, *Dalton Trans.* **2011**, *40*, 8922–8934.
[26] a) L. Dostál, R. Novák, R. Jambor, A. Růžička, I. Císařová, R. Jirásko, J. Holeček, *Organometallics* **2007**, *26*, 2911–2917; b) A. J. Arduengo III, C. A. Steward, *Chem. Rev.* **1994**, *94*, 1215–1237; c) A. J. Arduengo III, C. A. Steward, F. Davidson, D. A. Dixon, J. Y. Becker, S. A. Culley, M. B. Mizen, *J. Am. Chem. Soc.* **1987**, *109*, 627–647.
[27] a) A. Bondi, *J. Phys. Chem.* **1964**, *68*, 441–451; b) M. Mantina, A. C. Chamberlin, R. Valero, C. J. Cramer, D. G. Truhlar, *J. Phys. Chem. A* **2009**, *113*, 5806–5812.
[28] H. A. Bent, *Chem. Rev.* **1961**, *61*, 275–311.
[29] S. Grimme, *Angew. Chem. Int. Ed.* **2008**, *47*, 3430–3434; *Angew. Chem.* **2008**, *120*, 3478–3483.
[30] a) M. Ul-Haque, C. N. Caughlan, F. Ramirez, J. F. Pilot, C. P. Smith, *J. Am. Chem. Soc.* **1971**, *93*, 5229–5235; b) H. W. Roesky, V. W. Pogatzki, K. S. Dhathathreyan, A. Thiel, H. G. Schmidt, M. Dyrbusch, M. Noltemeyer, G. M. Sheldrick, *Chem. Ber.* **1986**, *119*, 2687–2697; c) T. Kawushima, K. Kato, R. Okazaki, *Angew. Chem. Int. Ed.* **1993**, *32*, 869–870; *Angew. Chem.* **1993**, *105*, 941–942; d) A. Chandrasekaran, R. O. Day, R. R. Holmes, *Inorg. Chem.* **2001**, *40*, 6229–6238; e) K. Kajiyama, M. Yoshimune, M. Nakamoto, S. Matsukawa, S. Kojima, K. Akiba, *Org. Lett.* **2001**, *3*, 1873–1875; f) S. Kojima, K. Kajiyama, M. Nakamoto, S. Matsukawa, K. Akiba, *Eur. J. Org. Chem.* **2006**, 218–234; g) K. Kajiyama, M. Yoshimune, S. Kojima, K. Akiba, *Eur. J. Org. Chem.* **2006**, 2739–2746; h) X.-D. Jiang, S. Matsukawa, H. Yamamichi, K. Kakuda, S. Kojima, Y. Yamamoto, *Eur. J. Org. Chem.* **2008**, 1392–1405; i) X.-D. Jiang, S. Matsukawa, K. Kakuda, Y. Fukuzaki, W–L. Zhao, L–S. Li, H.-B. Shen, S. Kojima, Y. Yamamoto, *Dalton Trans.* **2010**, 39, 9823–9829; j) L. J. Hounjet, C. B. Caputo, D. W. Stephan, *Angew. Chem. Int. Ed.* **2012**, *51*, 4714–4717; *Angew. Chem.* **2012**, *124*, 4792–4795.
[31] J. Bernstein, R. E. Davis, L. Shimoni, N.-L. Chang, *Angew. Chem. Int. Ed. Engl.* **1995**, *34*, 1555–1573.
[32] W. Koch, M. C. Holthausen, *A chemist's guide to density functional theory*, Wiley-VCH, New York, **2001**.
[33] C. Adamo, V. Barone, *J. Chem. Phys.* **1998**, *108*, 664–675.
[34] F. Weigend, R. Ahlrichs, *Phys. Chem. Chem. Phys.* **2005**, *7*, 3297–3305.

[35] T. H. Dunning, P. J. Hay, in *Methods of Electronic Structure Theory*, ed. H. F. Schaefer, Plenum Press, New York, **1977**, Vol. 2, p. 1.
[36] J. V. Ortiz, P. J. Hay, R. L. Martin, *J. Am. Chem. Soc.* **1992**, *114*, 2736–2737.
[37] A. E. Reed, R. B. Weinstock, F. Weinhold, *J. Chem. Phys.* **1985**, *83*, 735–746.
[38] F. A. Cotton, P. A. Kibala, *J. Am. Chem. Soc.* **1987**, *109*, 3308–3312.
[39] N. Bricklebank, S. M. Godfrey, A. G. Mackie, C. A. McAuliffe, R. G. Pritchard, *J. Chem. Soc. Chem. Commun.* **1992**, 355–356.
[40] M. C. Aragoni, M. Arca, F. Demartin, F. A. Devillanova, A. Garau, P. Grimaldi, F. Isaia, F. Lelj, V. Lippolis, G. Verani, *Eur. J. Inorg. Chem.* **2004**, 2363–2368.
[41] a) M. D. Rudd, S. V. Lindeman, S. Husebye, *Acta Chem. Scand.* **1997**, *51*, 689–708; b) M. C. Aragoni, M. Arca, F. Demartin, F. A. Devillanova, A. Garau, F. Isaia, F. Lelj, V. Lippolis, G. Verani, *Chem. Eur. J.* **2001**, *7*, 3122–3133; c) E. J. Juárez-Pérez, M. C. Aragoni, M. Arca, A. J. Blake, F. A. Devillanova, A. Garau, F. Isaia, V. Lippolis, R. Núñez, A. Pintus, C. Wilson, *Chem. Eur. J.* **2011**, *17*, 11497–11514.
[42] J. Tomasi, B. Mennucci, R. Cammi, *Chem. Rev.* **2005**, *105*, 2999–3093.

Manuscript received: May 10, 2022
Accepted manuscript online: July 12, 2022
Version of record online: August 26, 2022